Title. Mechanism of Action of KL-50, a Novel Imidazotetrazine for the Treatment of Drug-Resistant Brain Cancers.

Authors. Eric D. Huseman,[1] Anna Lo,[1] Olga Fedorova,[2,3] James L. Elia,[4] Susan E. Gueble,[5] Kingson Lin,[1,4,5] Ranjini Sundaram,[5] Danielle M. Burgenske,[6] Joonseok Oh,[1,7] Jinchan Liu,[1] Fabian Menges,[1,8] Matthew G. Rees,[9] Melissa M. Ronan,[9] Jennifer A. Roth,[9] Victor S. Batista,[1] Jason M. Crawford,[1,7,10] Jann N. Sarkaria,[6] Anna M. Pyle,[1,2,3] Ranjit S. Bindra,[4,5]* and Seth B. Herzon[1,5,11,]*

Affiliations:

[1]Department of Chemistry, Yale University; New Haven, Connecticut 06520, United States.

[2]Department of Molecular, Cellular, and Developmental Biology, Yale University; New Haven, Connecticut 06520, United States

[3]Howard Hughes Medical Institute; New Haven, Connecticut 06520, United States

[4]Department of Pathology, Yale School of Medicine; New Haven, Connecticut 06520, United States.

[5]Department of Therapeutic Radiology, Yale School of Medicine; New Haven, Connecticut 06520, United States.

[6]Department of Radiation Oncology, Mayo Clinic, Rochester, Minnesota.

[7]Institute of Biomolecular Design & Discovery, Yale University; West Haven, CT, United States

[8]Department of Chemistry, Chemical and Biophysical Instrumentation Center, Yale University; New Haven, Connecticut 06520, United States.

[9]Broad Institute of MIT and Harvard; Cambridge, MA 02142, Unites States

[10]Department of Microbial Pathogenesis, Yale School of Medicine; New Haven, Connecticut, United States

[11]Department of Pharmacology, Yale School of Medicine; New Haven, Connecticut 06520, United States.

Corresponding authors. Email: *ranjit.bindra@yale.edu; *seth.herzon@yale.edu

Abstract. Glioblastoma (GBM) is a lethal brain cancer with a five-year survival rate of <5%. Approximately half of GBM tumors lack the DNA repair protein O^6-methylguanine DNA methyltransferase (MGMT), which reverses O^6-alkylguanine (O^6G) lesions. Patients presenting MGMT– GBM are treated with surgery followed by radiation therapy and temozolomide (TMZ), an imidazotetrazine prodrug that produces O^6-methylguanine (O^6MeG) lesions. However, ~50% of these patients will develop TMZ resistance by silencing of the DNA mismatch repair (MMR) pathway. We recently reported that the novel N3-(2-fluoroethyl)imidazotetrazine "KL-50" is efficacious and well-tolerated in murine models of TMZ-resistant GBM (Lin et al. *Science* **2022**, *377*, 502). Herein, we rigorously establish that KL-50 generates DNA interstrand crosslinks (ICLs) by DNA alkylation to generate O^6-(2-fluoroethyl)guanine (O^6FEtG), displacement of fluoride to form an N1,O^6-ethanoguanine (N1,O^6EtG) intermediate, and ring-opening by the adjacent cytidine. 2-Chloroethylating agents, such as lomustine and mitozolomide (MTZ), generate the same ICL by an analogous mechanism. However, DNA ICLs form >10-fold more slowly from O^6FEtG than O^6ClEtG, and this slower rate of cross-linking allows MGMT to reverse the initial O^6FEtG in healthy tissue while also reducing MGMT–DNA cross-links arising from addition of MGMT to the N1,O^6EtG intermediate. KL-50 is efficacious in an intracranial patient-derived murine xenograft of TMZ-resistant, MGMT–/MMR– GBM (mOS = 205, 28, and 26 d for KL-50, TMZ, and vehicle-treated control, respectively) and in murine models of newly-diagnosed MGMT–/MMR+ GBM, suggesting its use in recurrent and up-front settings, respectively. These studies underscore the significance of considering the rates of chemical DNA modification and biochemical DNA repair in the design of systemic DNA alkylation agents.

INTRODUCTION

Approximately 20,000 people in the United States are diagnosed each year with glioblastoma (aka glioblastoma multiforme, GBM), an aggressive form of brain cancer.[1] The median survival following diagnosis is 1.2 years, and >95% of these patients will die within five years of presentation. Since 2005, the standard of care for GBM patients has consisted of surgical debulking followed by adjuvant radiotherapy and chemotherapy using the DNA methylating agent temozolomide (TMZ, **1**; Fig. 1a).[2,3] This treatment regimen provides a ~7 mo. survival benefit to patients harboring tumors that lack O^6-methylguanine-DNA-methyltransferase (MGMT; aka alkylguanine

transferase (AGT)), a DNA repair protein that reverses O^6-alkylguanine lesions (**5**), including the O^6-methylguanine (O^6MeG, **5a**) lesion derived from TMZ (**1**; vide infra). MGMT contains an active site cysteine residue that removes O^6 substituents from guanine by nucleophilic displacement (Fig. 1b).[4] The protein can accommodate a large degree of substitution at the O^6-position provided the carbon bonded to O^6 is a suitable substrate for a bimolecular displacement (e.g., methyl, primary, benzyl, or heteroarylmethyl).[5] *MGMT* is ubiquitously expressed in healthy tissue,[6] but, for reasons that are not fully understood, *MGMT* expression is lost in approximately half of GBMs by hypermethylation of CpG islands in the transcriptional promoter region of *MGMT*.[7] *MGMT* silencing also occurs in up to 70% of gliomas (lower grade brain cancers),[8] and in many non-central nervous system tumors, such as colon cancers,[9] melanomas,[10] non-small cell lung cancers,[11] and sarcomas,[12] among others (frequency of *MGMT* silencing ~20–50%). Consequently, MGMT expression levels have been used to predict tumor response to DNA alkylation agents.[7]

TMZ (**1**) is an imidazotetrazine prodrug developed by Stevens and co-workers and marketed under the trade name Temodar in the United States.[13] TMZ (**1**) is stable in the solid state or in acidic solution. However, in mildly basic solution it transforms to the triazene 3-methyl-(triazen-1-yl)-imidazole-4-carboxamide (MTIC, **2**) with a half-life ($t_{1/2}$) of 1.8 h at pH 7.4 and 37 °C (Fig. 1a).[14] MTIC (**2**) rapidly transforms to methyl diazonium (**3**; $t_{1/2}$ = 2 min at pH 7.4 and 37 ºC),[14] which is in equilibrium with diazomethane (**4**).[15] As expected based on this chemical mechanism, TMZ (**1**) is an indiscriminate methylating agent. Within DNA, N7-methylguanine (N7MeG, **8**) and N3-methyladenine (N3MeA, **9**) are the most abundant methylation products (70% and 9%, respectively)[16] but are readily-resolved by the base excision repair (BER) pathway and are not thought to contribute to the toxicity of TMZ (**1**; Fig. 1c).[17] Though O^6MeG (**5a**) constitutes only ~5% of the TMZ (**1**)-derived DNA methylation products, it is recognized as the clinically-significant site of alkylation.[13] O^6MeG (**5a**) is readily-reversed in tumors that express *MGMT* (referred to hereafter as "MGMT+" tumors). In MGMT-deficient tumors (referred to hereafter as "MGMT–" tumors), O^6MeG (**5a**) is mispaired with thymine (T) during replication (Fig. 1d). The resulting O^6MeG (**5a**)–T mismatch is recognized by the DNA mismatch repair (MMR) pathway. MMR resects the mispaired thymine and adjacent nucleotides, creating a gap (Fig. 1e). However, the orphaned O^6MeG (**5a**) is again mispaired with thymine during replication. These cycles of MMR-dependent thymine resection and polymerase-dependent thymine insertion (referred to as "futile cycling" in the GBM literature)[18] lead to DNA double-strand breaks (DBSs) and, ultimately, apoptosis.

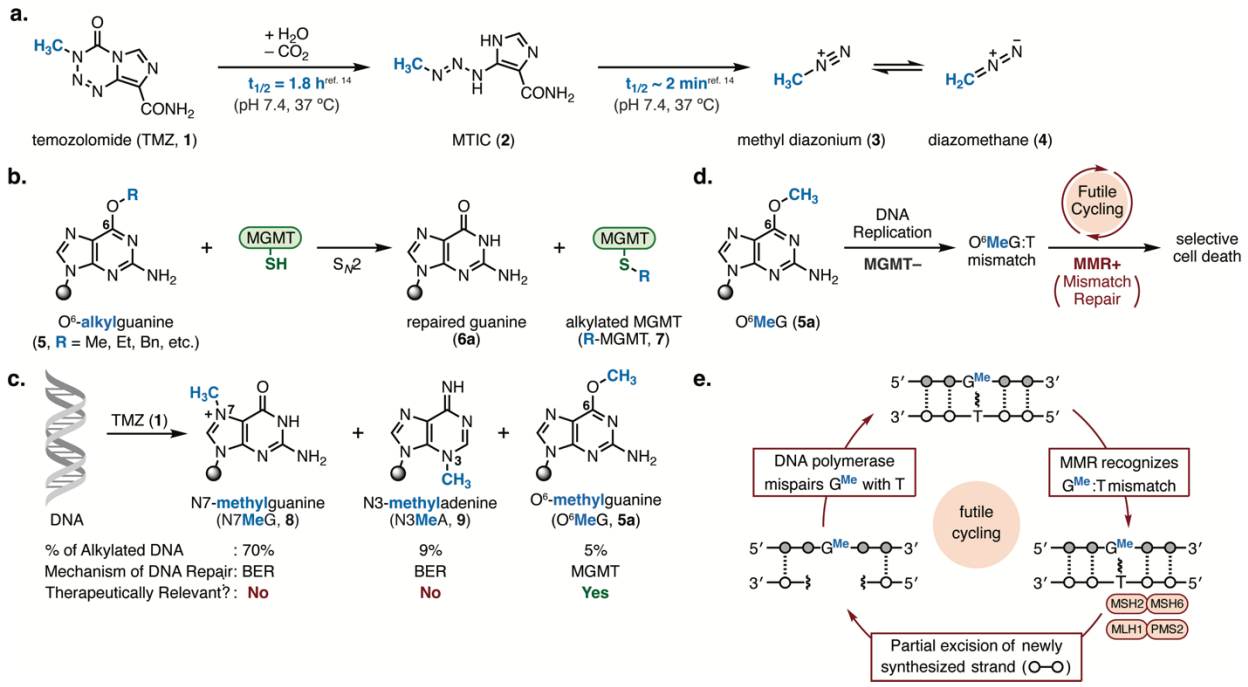

Fig. 1. a. Spontaneous hydrolytic decomposition of temozolomide (TMZ, **1**) under physiological conditions generates 3-methyl-(triazen-1-yl)-imidazole-4-carboxamide (MTIC, **2**) which further degrades to the alkylating agent methyl diazonium (**3**), which is in equilibrium with diazomethane (**4**). **b.** The DNA repair protein O^6-methylguanine-DNA-methyltransferase (MGMT) repairs O^6-alkylguanine lesions (**5**) by S_N2 displacement using

an active site cysteine residue (Cys145) as a nucleophile. The resulting alkylated MGMT **7** is ubiquitinated and degraded by the proteosome. **c.** Alkylation of DNA by TMZ (**1**) yields a mixture of methylation products. O^6MeG (**5a**) is the clinically-significant DNA alkylation product. **d.** In the absence of MGMT, O^6MeG (**5a**) lesions enter DNA replication and are mispaired with thymine leading to activation of the mismatch repair pathway (MMR), futile cycling, and, eventually, cell death. **e.** Overview of the mechanism of futile cycling.

Most patients harboring MGMT– GBM respond initially to TMZ (**1**), but ~50% of these patients (or, ~25% of all GBM patients), as well as >50% of all patients with recurrent lower grade gliomas, acquire resistance to TMZ (**1**) by downregulation or inactivation of MMR activity.[19] The resulting MGMT–, MMR-deficient tumors (referred to hereafter as "MGMT–/MMR–" tumors) proliferate with O^6MeG (**5a**) in their genome and are unresponsive to further TMZ (**1**) treatment. The mispairing of O^6MeG (**5a**) with thymine in these cells leads to nucleotide transitions, resulting in tumors with a "hypermutator phenotype" that are frequently more aggressive than those that have not been challenged with TMZ (**1**).[19b]

No effective treatments are available for recurrent MGMT–/MMR– GBM. Many patients receive 1-(2-chloroethyl)-3-cyclohexyl-1-nitrosourea (aka lomustine or CCNU, **10**; marketed under the trade name Gleostine; Fig. 2a).[20] However, the benefits of this therapy are limited and 80% of patients will progress within 6 months of beginning lomustine (**10**) treatment (see also Fig. 6 and associated text).[21] Lomustine (**10**) is a prodrug that transfers a 2-chloroethyl substituent to O^6-guanine to form O^6-(2-chloroethyl)guanine (O^6ClEtG, **5b**). These O^6ClEtG (**5b**) lesions evolve to the [G(N1)–C(N3)]Et DNA interstrand crosslink (ICL) **14a** by a two-step pathway comprising unimolecular displacement of chloride to form the N1,O^6-ethanoguanine (N1,O^6EtG) intermediate **12a** and ring-opening (with C–O bond cleavage) by the adjacent cytidine residue (**13a**; Fig. 2b).[22] As cell death via DNA ICLs does not depend on mismatch repair, lomustine (**10**) is toxic to MGMT–/MMR– cells.[23] However, as demonstrated in our previous study,[24] MGMT provides a smaller degree of protection from lomustine (**10**) than it does for TMZ (**1**). In short-term growth delay assays, the therapeutic indices (defined as the IC_{50} in LN229 GBM MGMT+/MMR+ cells divided by the IC_{50} in LN229 GBM MGMT–/MMR+ cells) of lomustine (**10**) and TMZ (**1**) were 3.4 and 89, respectively. This is consistent with clinical data wherein off-target toxicity limits the dosing of lomustine (**10**).[25] Mitozolomide (MTZ, **11**) is an N3-(2-chloroethyl)imidazotetrazine that advanced to clinical trials but was abandoned due to toxicity.[26] Though the mechanism of action of MTZ (**11**) has not been rigorously established, it transfers a 2-chloroethyl substituent to DNA and likely cross-links DNA by a pathway analogous to lomustine (**10**; Fig. 2b).[27] Consistent with this, we found that MTZ (**11**) exhibited a smaller therapeutic index than TMZ (**1**) (6.9 vs. 89, respectively).[24]

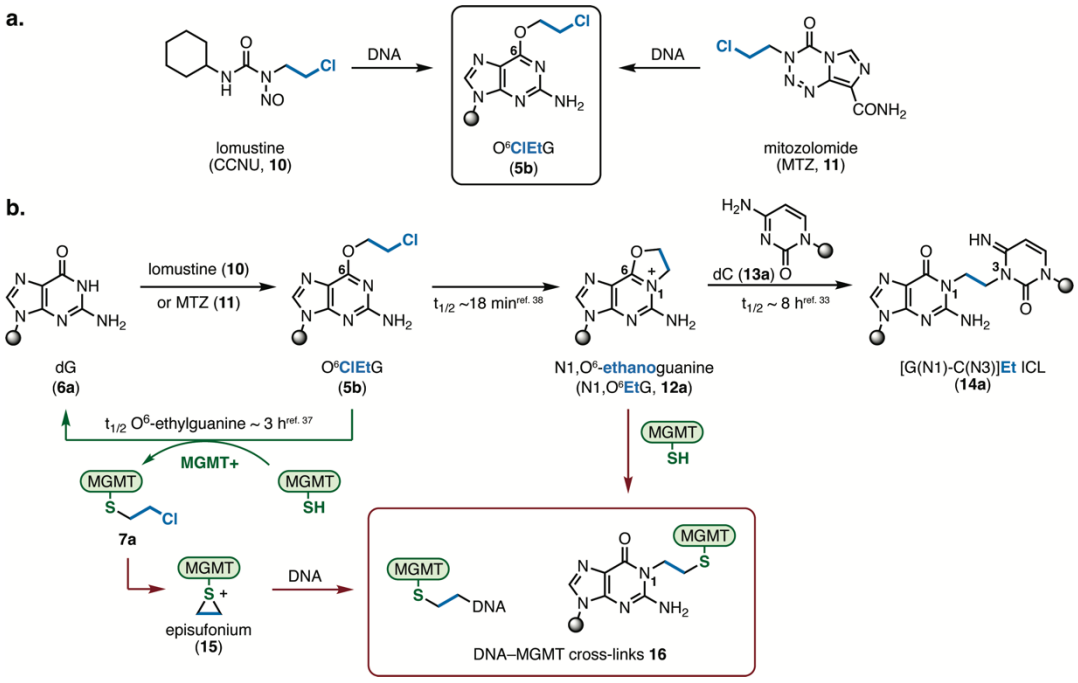

Fig. 2. Alkylation at O^6-guanine by lomustine (aka CCNU, **10**) leads to the formation of toxic [G(N1)–C(N3)]Et DNA interstrand crosslinks (ICLs, **14a**) in MGMT– cell lines. Though the mechanism of MTZ (**11**) has not been rigorously established, it is likely that it follows a parallel pathway. **a.** Lomustine (**10**) and MTZ (**11**) generate O^6-(2-chloroethyl)guanine (O^6ClEtG, **5b**) lesions. **b.** O^6ClEtG (**5b**) evolves to the ICL **14a** by unimolecular displacement of chloride to form N1,O^6-ethanoguanine (N1,O^6EtG, **12a**) followed by ring-opening by the adjacent cytidine base (**13a**). Under physiological conditions, the half-lives for the transformations **5b→12a** and **12a→14a** are 18 min and 8 h, respectively. The rate of MGMT reversal of O^6ClEtG (**5b**) is not known, but the half-life of O^6-ethylguanine is 180 min in vivo. Collectively, these rate data suggest that N1,O^6EtG (**12a**) accumulates in MGMT+ cells. Ring-opening of N1,O^6EtG (**12a**) by MGMT generates the DNA–MGMT crosslink **16**. Alternatively, MGMT reversal of O^6ClEtG (**5b**) forms the 2-chloroethylsulfide **7a** that may crosslink to DNA via the episulfonium ion intermediate **15**. We hypothesize that these DNA–MGMT crosslinks drive the dose-limiting toxicity of lomustine (**10**) and MTZ (**11**) in MGMT+ cells.

We hypothesized that an alkylating agent that retained lomustine (**10**) and MTZ's (**11**) ability to form DNA ICLs but increased the ability of MGMT to mitigate toxicity to healthy MGMT+ tissues might prove effective against recurrent, TMZ (**1**)-resistant MGMT–/MMR– GBM. In researching this hypothesis, we noted studies with normal (IMR-90, MGMT+) and SV40-transformed (VA-13, MGMT–) human embryo cells that seemed to suggest DNA ICL formation is not the driver of lomustine (**10**) and MTZ (**11**) toxicity in the MGMT+ cell line.[27a, 28] Specifically, these studies showed that though the toxicity of lomustine (**10**) and MTZ (**11**) increased in a dose-dependent manner in both cell lines, only the MGMT– VA-13 cell line showed a dose-dependent increase in ICL formation.[29] While one could theoretically attribute the toxicity of lomustine (**10**) in this MGMT+ setting to protein carbamoylation by the cyclohexyl isocyanate liberated upon its decomposition,[30] this pathway of toxicity is not operative for MTZ (**11**) as it has no carbamoylating activity.[31]

Brent and coworkers reported that the addition of partially-purified human MGMT to DNA treated with the O^6-2-chloroethylating agent 1,3-bis(2-chloroethyl)-1-nitrosourea (BCNU) led to the formation of covalent DNA–MGMT crosslinks.[32] Pretreatment of MGMT with O^6MeG (**5a**)-containing DNA decreased DNA–MGMT crosslinks,[32b] indicating that the active site cysteine residue (Cys145), required for O^6-alkylguanine repair, is also responsible for DNA protein crosslink (DPC) formation. Brent and coworkers provided further evidence for nucleophilic cysteinyl sulfur attack by determining that the covalent DNA–MGMT linkage occurred between the N1 position of guanine and an MGMT cysteine sulfur, with an intervening two-carbon linker.[33] This connectivity suggests that DNA–MGMT crosslinks arise from ring-opening of N1,O^6EtG (**12a**) by MGMT (Fig. 2b). This mechanistic hypothesis is substantiated by the fact that the kinetics for the loss of capacity to form DNA–MGMT crosslinks mirrors that of the formation of the ICL **14a**.[33]

While the clinical significance of these DPCs is currently unknown, evidence suggests MGMT–DNA crosslinks are toxic. For example, expression of human MGMT in *Escherichia coli* strains lacking endogenous MGMT increases the toxicity of 1,2-dibromoethane by the formation of DNA–MGMT crosslinks.[34] These DNA–MGMT crosslinks form by initial alkylation of the MGMT active site cysteine to generate a bromoethyl sulfide which evolves to the episulfonium **15**. This electrophilic intermediate alkylates DNA at various sites resulting in the formation of ethyl-linked DNA–MGMT crosslinks at N1G, N^2G, O^6G, N7G, and N^6-adenine (N^6A), with the N7G adduct predominating.[35] Additionally, electroporation of 2-hydroxyl-3,4-epoxybutane-modified MGMT into mammalian cells led to the formation of DNA–MGMT crosslinks at N7G and increased cytotoxicity as compared to control.[36]

These data suggest that DNA–MGMT crosslinks contribute to the toxicity of lomustine (**10**) and MTZ (**11**) in MGMT+ cells. Examination of the chemical kinetics for MGMT repair of O^6ClEtG (**5b**), evolution of O^6ClEtG (**5b**) to N1,O^6EtG (**12a**), and capture of **12a** by the base-paired cytidine (**13a**) to yield ICL **14a** bolster this hypothesis. The rate of MGMT reversal of O^6ClEtG (**5b**) has not been measured (likely due the instability of this base toward N1,O^6EtG formation), but the half-life of O^6-ethylguanine toward MGMT reversal is ~180 min in vivo under pseudo-first order conditions.[37] In contrast, O^6ClEtG (**5b**) evolves to N1,O^6EtG (**12a**) with a half-life of 18 min at pH 7.4 and 37 °C based on model studies with the ribonucleoside O^6-(2-chloroethyl)guanosine (**5d**; Fig. 3, vida infra).[38] Finally, N1,O^6EtG (**12a**) has a half-life of ~8 h toward ring-opening by the adjacent cytidine base (**12a→14a**, Fig. 2b).[33] Taken collectively, these rate data make it clear that N1,O^6EtG (**12a**) accumulates in MGMT+ cells exposed to lomustine (**10**) or MTZ (**11**), likely leading to DNA–MGMT crosslinks in healthy tissue. Furthermore, we posit that the chloroethyl sulfide **7a** formed by MGMT reversal of O^6ClEtG (**5b**) could form the

episulfonium **15** and produce DNA–MGMT crosslinks by a mechanism analogous to 1,2-dibromoethane-induced DNA–MGMT crosslinks (vide supra).[34]

We reasoned that slowing the rate of formation of N1,O^6EtG (**12a**) without attenuating the rate of MGMT reversal of the initial O^6-guanine alkylation product might decrease the amount of DNA–MGMT DPCs in healthy tissue and, ultimately, lead to an agent effective against recurrent, MGMT–/MMR– GBM. If the rate of N1,O^6EtG (**12a**) formation was slowed by decreasing the leaving group ability of the distal substituent, one would anticipate the episulfonium ion crosslinking pathway (**7a→16**; Fig. 2b) might also be diminished. We focused on derivatives of temozolomide (**1**) owing to its clinical use in glioblastoma therapy. Additionally, the cyclohexyl isocyanate liberated upon decomposition of lomustine (**10**) is known to induce toxicity via protein carbamoylation,[39] and this pathway is not possible with imidazotetrazine derivatives.[31] These studies led to the identification of the N3-(2-fluoroethyl)imidazotetrazine KL-50 (**19**, Fig. 4) as the first reported compound to overcome acquired TMZ (**1**) resistance while maintaining high selectivity for MGMT– cells.[24] KL-50 (**19**) is efficacious and well-tolerated in in vivo models of drug-resistant GBM, including a murine intracranial xenograft of a patient-derived, drug-resistant (MGMT–/MMR–) tumor presented below.

Herein, we elucidate the mechanism of action of KL-50 (**19**). Consistent with the analysis outlined above, our data suggest that the superior efficacy of this compound derives from slower rates of DNA ICL formation and a near complete elimination of DNA–MGMT crosslinks, which allows one to achieve efficacious concentrations of drug without toxicity to healthy (MGMT+) cells. This compound is currently being developed by Modifi Biosciences for the treatment of newly diagnosed and recurrent, TMZ (**1**)-resistant GBM. Broadly, this study underscores the importance of considering the elementary steps of DNA chemical modification and biochemical DNA repair in designing genotoxic chemotherapeutic agents targeting specific tumor-associated DNA repair defects.

RESULTS

In accord with the mechanistic analysis outlined above, we designed and synthesized a series of N3-(2-heteroethyl)imidazotetrazine derivatives with poor leaving groups at the distal position of the two-carbon chain. We were motivated to synthesize KL-50 (**19**) in part by a report that O^6-(2-fluoroethyl)guanosine (**5c**) transforms to the N1,O^6-ethanoguanosine **12b** with a half-life of 18.5 h at pH 7.4 and 37 °C[40]; by comparison, the half-life of O^6-(2-chloroethyl)guanosine (**5d**) is 18 min under similar conditions (Fig. 3).[38] While nucleophilic displacement of fluoride is unusual, many instances of unimolecular displacement of an aliphatic fluoride by an appropriately-positioned nucleophile have been documented (often as problematic degradation pathways) in the pharmaceutical literature.[41] There is little doubt that such substitutions are accelerated in aqueous environments by hydrogen bonding to fluoride in the transition state for displacement. Assuming the rate of MGMT reversal of O^6-(2-fluoroethyl)guanine (O^6FEtG, **5e**; see Fig. 9a below) is comparable to that of O^6-ethylguanine (see Fig. 2b), O^6FEtG (**5e**) would appear to satisfy the mechanistic objectives discussed above. Additionally, there is evidence in the literature that the fluorine substituent might stabilize, to some extent, the expected 2-fluoroethyldiazonium intermediate.[42] Though KL-50 (**19**) is a simple change from TMZ (**1**) and MTZ (**11**), it does not appear to have been previously synthesized, though it does appear prophetically in a patent.[43] The synthesis of KL-50 (**19**) follows that developed by Ege and Gilbert[44] and Stevens,[45] and proceeds by diazotization of commercially available 5-aminoimidazole-4-carboxamide hydrochloride (**18**) followed by formal cycloaddition with 2-fluoroethyl isocyanate (23% overall, Fig. 4). The structure of KL-50 (**19**) was established by NMR, HRMS, and single crystal X-ray diffraction (CCDC #2122008/2122009) analyses.

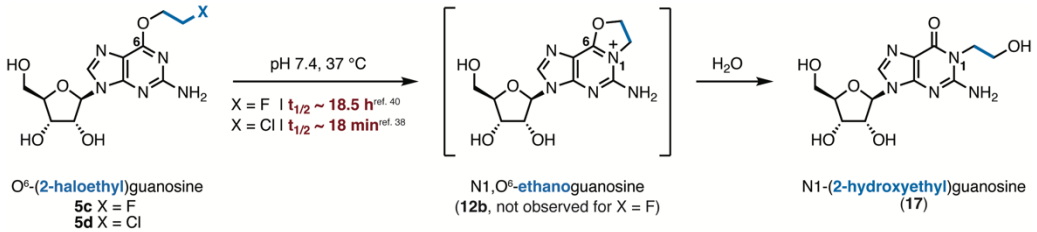

Fig. 3. Conversion of O^6-(2-fluoroethyl)guanosine (**5c**) and O^6-(2-chloroethyl)guanosine (**5d**) to N1-(2-hydroxyethyl)guanosine (**17**) proceeds with half-lives of 18.5 h and 18 min, respectively, under physiological conditions.

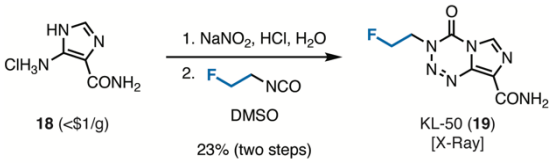

Fig. 4. Synthesis of KL-50 (**19**).

We evaluated the activity of TMZ (**1**), KL-50 (**19**), lomustine (**10**) and MTZ (**11**) in long-term clonogenic survival assays (Fig. 5). We employed four isogenic LN229 GBM cell lines engineered to be proficient or deficient in MGMT and/or MMR.[24] The use of an isogenic panel provides a robust correlation between DNA repair activity and cellular phenotype.[46] As anticipated, TMZ (**1**) was efficacious against MGMT–/MMR+ cell lines but not MGMT+/MMR± or MGMT–/MMR– lines (Fig. 5a). On the other hand, KL-50 (**19**) displayed highly selective toxicity toward MGMT– cells, regardless of MMR status. We observed surviving fractions of 6.3×10^{-4} and 4.0×10^{-5} in MGMT–/MMR+ and MGMT–/MMR– cell lines, respectively, treated with 30 μM KL-50 (**19**; Fig. 5b); in contrast, MGMT+ cells proved highly resistant to KL-50 (**19**) as we only observed ~60–70% cell kill at 200 μM KL-50 (**19**). Thus, KL-50 (**19**) is $>10^4$-fold more potent toward MGMT– cell lines than MGMT+ cell lines. In contrast, while lomustine (**10**) eradicated the growth of MGMT– cell lines irrespective of MMR status, we observed significant toxicity toward MGMT+ cell lines (Fig. 5c). For example, the surviving fractions of MGMT+/MMR+ and MGMT+/MMR– cells treated with 200 μM lomustine (**10**) were $<10^{-4}$ and $<10^{-3}$, respectively. As expected, MTZ (**11**) was also toxic to MGMT+ cells at high concentrations (Fig. 5d). Taken together, these assays establish KL-50 (**19**) as highly efficacious in MGMT– GBM cell lines irrespective of MMR status, while the profiles of

lomustine (**10**) and MTZ (**11**) in this assay are consistent with the lower tolerability of these reagents deriving from toxicity to healthy MGMT+ cell lines.

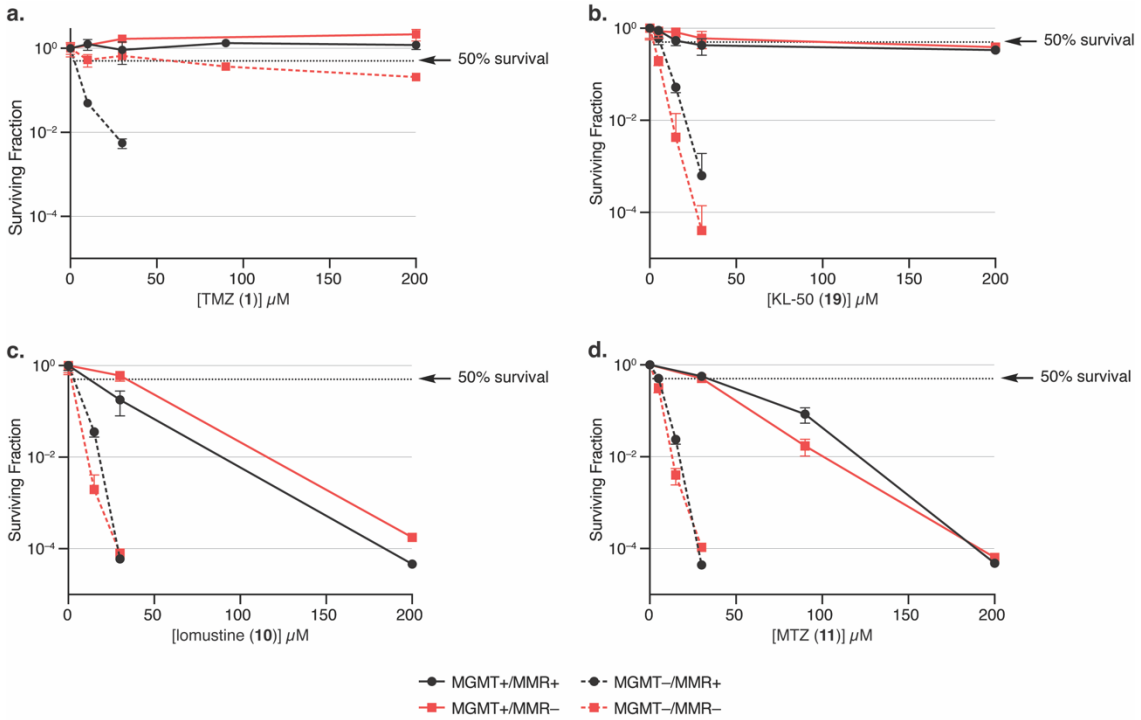

Fig. 5. Long-term clonogenic survival assays evaluating TMZ (**1**, panel **a**), KL-50 (**19**, panel **b**), lomustine (**10**, panel **c**), or MTZ (**11**, panel **d**) in isogenic glioblastoma LN229 cells proficient or deficient in MGMT and MMR. Solid series: MGMT-proficient (MGMT+) cell lines. Dashed series: MGMT-deficient (MGMT–) cell lines. Black circle series: MMR-proficient (MMR+) cell lines. Red square series: MMR-deficient (MMR–) cell lines. A dashed line corresponding to 50% cell survival is indicated by an arrow in each panel. Points indicate mean; error bars indicate standard deviation; n ≥ 3 technical replicates.

To further probe the cell line selectivity of KL-50 (**19**), we evaluated its activity at seven dosages (91 nM–200 μM) against 902 human cancer cell lines using the high-throughput PRISM (Profiling Relative Inhibition Simultaneously in Mixtures) screen (Fig. 6).[47] Comparison of toxicity, as measured by area under the curve (AUC), a metric that captures toxicity across the entire dosage range, to levels of *MGMT* expression showed a high Pearson's correlation coefficient (r = 0.642), indicating that there is a strong positive correlation between MGMT gene expression and cell viability across all cell lines assayed. This is comparable in magnitude to Pearson correlations observed for the BCL2 inhibitor venetoclax vs. *BCL2* expression (r = –0.590), the EGFR inhibitor erlotinib vs. *EGFR* expression (r = –0.358), and the TOP2α inhibitor etoposide vs. *TOP2α* expression (r = –0.185) based upon AUC data obtained in similar[47b] screens from the Wellcome Sanger Institute's Genomics of Drug Sensitivity in Cancer project (Fig. S1).[48] This correlation analysis of cell viability vs. gene expression for ~19,000 protein-coding genes was conducted for all seven doses of KL-50 (**19**) as well as the AUC and IC_{50}. These analyses are summarized in Fig. 6b in which each point represents one correlation analysis plotted as a function of its Pearson correlation (r) and its false discovery rate (q-value). MGMT expression was uniquely correlated with viability (see also Fig. S2). Finally, we binned the cell lines into low and high MGMT expressing groups in which the low MGMT group represents the lowest ~16% of MGMT expressors (i.e., cells having MGMT expression >1 standard deviation below the mean) and the high MGMT group represents all other cell lines (Fig. 6c). As expected, the low MGMT group demonstrated statistically lower viability as measured by AUC as compared to the high MGMT group ($p < 0.0001$). Taken together, these data corroborate the selectivity of KL-50 (**19**) for MGMT–cells first observed in LN229 GBM cells across a much larger array of cancer cell lines.

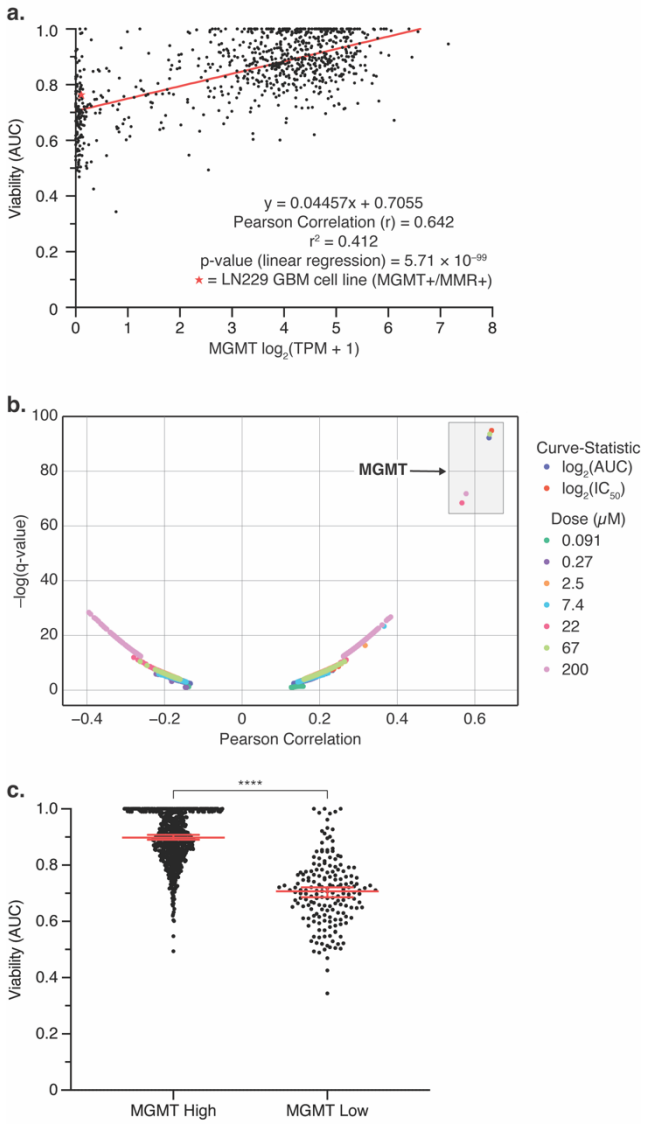

Fig. 6. PRISM multiplexed viability screen with KL-50 (**19**) across a library of 902 Cancer Cell Line Encyclopedia (CCLE) cell lines. **a**. Example of individual correlation analysis shown for *MGMT* gene expression vs. KL-50 (**19**) AUC. Each point represents a different cell line. AUC values range from 0 to 1 with AUC = 0 and 1 representing 0% and 100% cell survival, respectively, across all drug doses. TPM = transcripts of MGMT per 1 million transcripts. **b.** Correlation analysis of gene expression vs. drug response across IC_{50}s, AUCs, and various individual concentrations of KL-50 (**19**) in the PRISM platform. Each point represents an individual correlation analysis as show in panel **a**. For each point, the false discovery rates (q-values) were computed from p-values using the Benjamini–Hochberg algorithm. Associations with q-values above 0.1 were filtered out, and only the top 500 genes at each dose are visualized. Boxed associations indicate, with high confidence, that MGMT gene expression is highly correlated with KL-50 (**19**) resistance across a wide concentration range. See Fig. S2 for lists of top 10 genes ranked by Pearson Correlation and q-value. **c.** Scatter dot plot displays cell viability as measured by AUC for MGMT High (mRNA z-score >–1, n = 664) and MGMT Low (mRNA z-score <–1, n = 180) cell lines. Lines indicate median; error bars indicate 95% confidence interval; **** $p < 0.0001$.

In our earlier publication we carried out a preliminary evaluation of the in vivo efficacy of KL-50 (**19**) in murine flank and intracranial models of MGMT–/MMR– GBM tumors.[24] In an intracranical model, KL-50 (**19**) was highly efficacious against TMZ-resistant MGMT–/MMR– tumors using different doses (5, 15 or 25 mg/kg), dosing schedules (MWF for 3 weeks or M–F for 1 week), or routes of administration (oral or intraperitoneal). KL-50 (**19**) reduced the growth of large flank tumors (~350 to 400 mm^3), and it diminished MGMT–/MMR+ GBM tumors, a model for newly-diagnosed GBM. Hematological profiling revealed blood counts (white blood cells, neutrophils,

lymphocytes, red blood cells, and platelets) in the normal range (defined as values falling within two standard deviations of the average for healthy mice) when dosing up to 100 mg/kg KL-50 (**19**). To further illustrate the potential of KL-50 (**19**) for application in recurrent MGMT–/MMR– GBM in the clinical setting, we evaluated the efficacy of KL-50 (**19**) in a patient-derived intracranial xenograft of MGMT–/MMR– GBM. This tumor was derived from a patient that presented with an MGMT–/MMR+ tumor. Following biopsy, the cell line was exposed in vivo to cyclical doses of TMZ (**1**; 50 mg/kg) to induce MMR-based resistance. Western blotting revealed that the resulting resistant cell line (GBM12TMZ subline 8023) lacked expression of the MMR repair protein MSH6. We evaluated TMZ (**1**) and lomustine (**10**) in the same model for comparison. Both were dosed at 0.1 mg/dose (5 mg/kg for a 20 g mouse), p.o., q.d., every 7 d, for 3 cycles. As shown in Fig. 7a, neither TMZ (**1**) nor lomustine (**10**) provided a significant survival benefit (median overall survival (mOS) = 30 d, 28 d, and 26 d for lomustine (**10**), TMZ (**1**), and vehicle, respectively). By comparison, KL-50 (**19**) dosed at 25 mg/kg, p.o., q.d., for 5 d every 28 d for 3 cycles provided a >6-fold increase in median mOS (205 d) as compared to vehicle (mOS = 28 d) and TMZ (**1**, mOS = 29 d), Fig 7b).

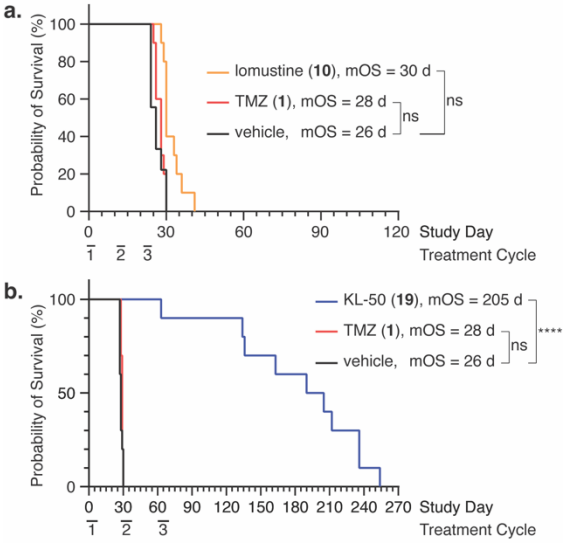

Fig. 7. Kaplan–Meier survival curves from an intracranial model evaluating the efficacy of KL-50 (**19**) in the patient-derived MGMT–/MMR– GBM cell line GBM12TMZ subline 8023. **a.** Lomustine (**10**), which is used clinically in recurrent, MGMT–/MMR– GBM, provides only a marginal survival benefit. Dosing schedule: 0.1 mg/dose (5 mg/kg for a 20 g mouse), p.o., q.d., every 7 d, 3 cycles. **b.** KL-50 (**19**) provides a >6-fold increase in median overall survival (mOS). Dosing schedule: 25 mg/kg, p.o., q.d., for 5 d every 28 d, 3 cycles. **** $p < 0.0001$; ns, not significant.

As outlined above, we hypothesized that KL-50 (**19**) would generate DNA ICLs (**14a**) by unimolecular displacement of fluoride to form N1,O^6EtG (**12a**) and ring-opening by the based-paired cytidine residue (**13a**; see Fig. 9a). Because fluoride displacement is rare (but not unprecedented, vide supra) we sought to rigorously probe for ICL formation in tissue culture samples treated with KL-50 (**19**). We previously employed a modification of the well-known alkaline comet assay to probe for production of DNA ICLs.[24, 49] In this assay, LN229 MGMT–/MMR± cells were treated with drug, washed, spread on comet slides, and lysed. The lysed cells were exposed to 0 or 10 Gy of ionizing radiation and subjected to alkaline unwinding electrophoresis. DNA was then imaged and quantified by fluorescence following staining with SYBR gold. Smaller fragments of DNA arising from ionizing radiation-induced breaks migrate with higher mobility in the alkaline electrophoresis, leading to the characteristic "comet tail". In contrast, pretreatment with DNA crosslinking agents abrogates the ionizing radiation-induced tailing, leading to a reduction in the amount of DNA in the tail. These initial studies showed that KL-50 (**19**) treatment reduced the %DNA in the tail as compared to control, consistent with DNA ICL formation.

To determine if MGMT can rescue cells from DNA ICL formation by KL-50 (**19**), we performed this assay across the full panel of isogenic LN229 MGMT±/MMR± cell lines (Fig. 8a). We found that KL-50 (**19**) only reduced %DNA in the tail in the MGMT–/MMR± cell lines, indicating that KL-50 (**19**) does not form DNA ICLs in the presence of MGMT. This mirrors the lack of ICL formation observed for the 2-chloroethylation agents

lomustine (**10**) and MTZ (**11**) in MGMT+ IMR-90 human embryo cells as noted above.[27a, 28] As an orthogonal probe of ICL formation, we isolated genomic DNA from LN229 MGMT±MMR± cells treated with 200 µM KL-50 (**19**), MTZ (**11**), or TMZ (**1**) for 24 h and analyzed the DNA by denaturing electrophoresis (Fig. 8b). We observed cross-linking by KL-50 (**19**) only in MGMT– cell lines.

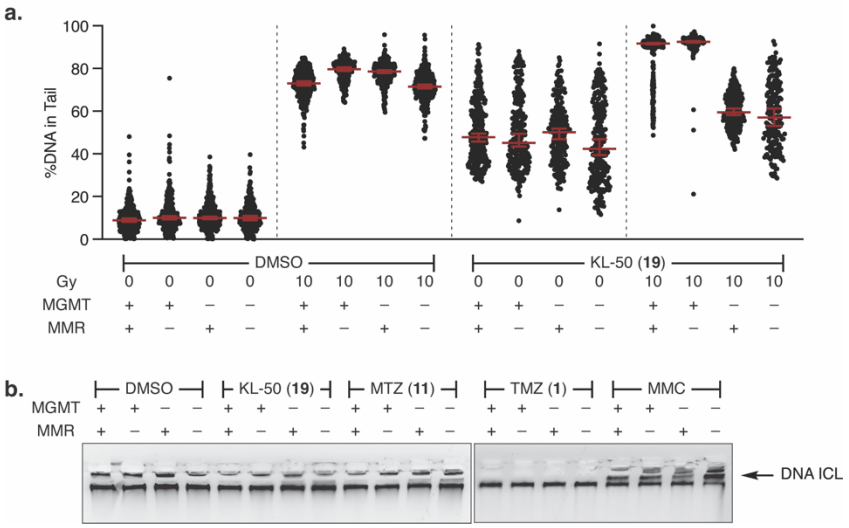

Fig. 8. KL-50 (**19**) only induces DNA ICLs in the absence of MGMT. **a.** Modified alkaline comet assay performed on LN229 MGMT±/MMR± cells treated with 0.1% DMSO control or KL-50 (**19**, 200 µM) for 24 h. **b.** Denaturing gel electrophoresis of genomic DNA isolated from LN229 MGMT±/MMR± cells treated with DMSO control, KL-50 (**19**, 200 µM), MTZ (**11**, 200 µM), or TMZ (**1**, 200 µM) for 24 h or mitomycin C (MMC, 50 µM) for 2 h. Bands indicating crosslinked DNA are indicated by the arrow.

We previously described the time-dependent induction of cellular markers of DNA replication stress and DNA double-strand breaks (DSBs) by KL-50 (**19**) in an MGMT-dependent, MMR-independent manner.[24] We also demonstrated that KL-50 (**19**) activates the Fanconi anemia (FA) DNA interstrand crosslink repair pathway,[50] as measured by FANCD2 ubiquitination, and induces cell cycle arrest, primarily in MGMT-deficient cells. Further supporting the induction of ICLs and eventual conversion to DSBs as a mechanism of KL-50 (**19**) toxicity, we found that homologous recombination repair-deficient (BRCA2–/–) and FA pathway deficient (FANCD2–/–) cell lines display hypersensitivity to KL-50 (**19**) in the absence of MGMT. Finally, an examination of alternative mechanisms of action suggested that BER, nucleotide excision repair (NER), reactive oxygen species (ROS), and DNA destabilization are peripheral or noncontributory to the mechanism of action of KL-50 (**19**).

We carried out in vitro alkylation studies to more closely evaluate the structure of the ICLs derived from KL-50 (**19**). By analogy to lomustine (**10**) and MTZ (**11**), we anticipated that treatment of DNA with KL-50 (**19**) would result in the initial formation of O^6FEtG (**5e**) lesions that would evolve to the [G(N1)–C(N3)]Et ICL (**14a**; Fig. 9a). As such, in vitro DNA alkylation followed by enzymatic digestion should yield a pool of nucleosides containing O^6-(2-fluoroethyl)-2′-deoxyguanosine (O^6FEtdG, **5f**) and the [dG(N1)-dC(N3)]Et ICL (**14b**; Fig. 9b). We initiated these studies by synthesizing the requisite deoxynucleosides **5f** and **14b** (Fig. S2). Though both **5f**[51] and **14b**[22, 51-52] have been previously described, to the best of our knowledge, detailed spectroscopic data have not been reported for either compound. The Supporting Information of this manuscript contains detailed experimental procedures for the preparation of **5f** and **14b** and complete NMR and high-resolution mass spectrometry (HRMS) characterization data for each compound (Figs. S3–S9). Comparison of experimental carbon-13 NMR shifts of synthetic **14b** to theoretical carbon-13 NMR shifts of **14b** as well as three additional [dG-dC]Et ICL isomers (**S1–S3**) in combination with 2-D NMR data (Figs. S6–S8) provide further support for the UV spectroscopy-based structural assignment of the [dG(N1)-dC(N3)]Et ICL (**14b**) by Ludlum and coworkers in 1982.[22]

With the required synthetic standards in hand, calf thymus DNA (4 mg/mL) was incubated with KL-50 (**19**, 1 mM) for 5 or 72 h at 37 ºC (Fig. 9b). Following removal of small molecules by size exclusion spin filtration, the alkylated

DNA was digested with exonuclease III, exonuclease T5, and QuickCIP phosphatase. Analysis of the resulting nucleoside mixtures using liquid chromatography (LC) combined with HRMS showed the presence of O^6FEtdG (**5f**) after 5 and 72 h while the [dG(N1)-dC(N3)]Et ICL (**14b**) was only observed only after 72 h (Fig. 9c–e). The structures of these products were verified by targeted LC/MS/MS by comparison with the synthetic standards (Figs. S10–S15). Neither O^6FEtdG (**5f**) nor the [dG(N1)-dC(N3)]Et ICL (**14b**) was observed in control experiments in which calf thymus DNA was treated with vehicle for 5 or 72 h at 37 ºC. These results are consistent with initial formation of an O^6FEtG lesion (**5e**) in DNA that evolves to the [G(N1)-C(N3)]Et ICL (**14a**) in a manner analogous to the O^6ClEtG DNA lesion formed by lomustine (**10**) and MTZ (**11**; compare Figs. 2b and 9a).

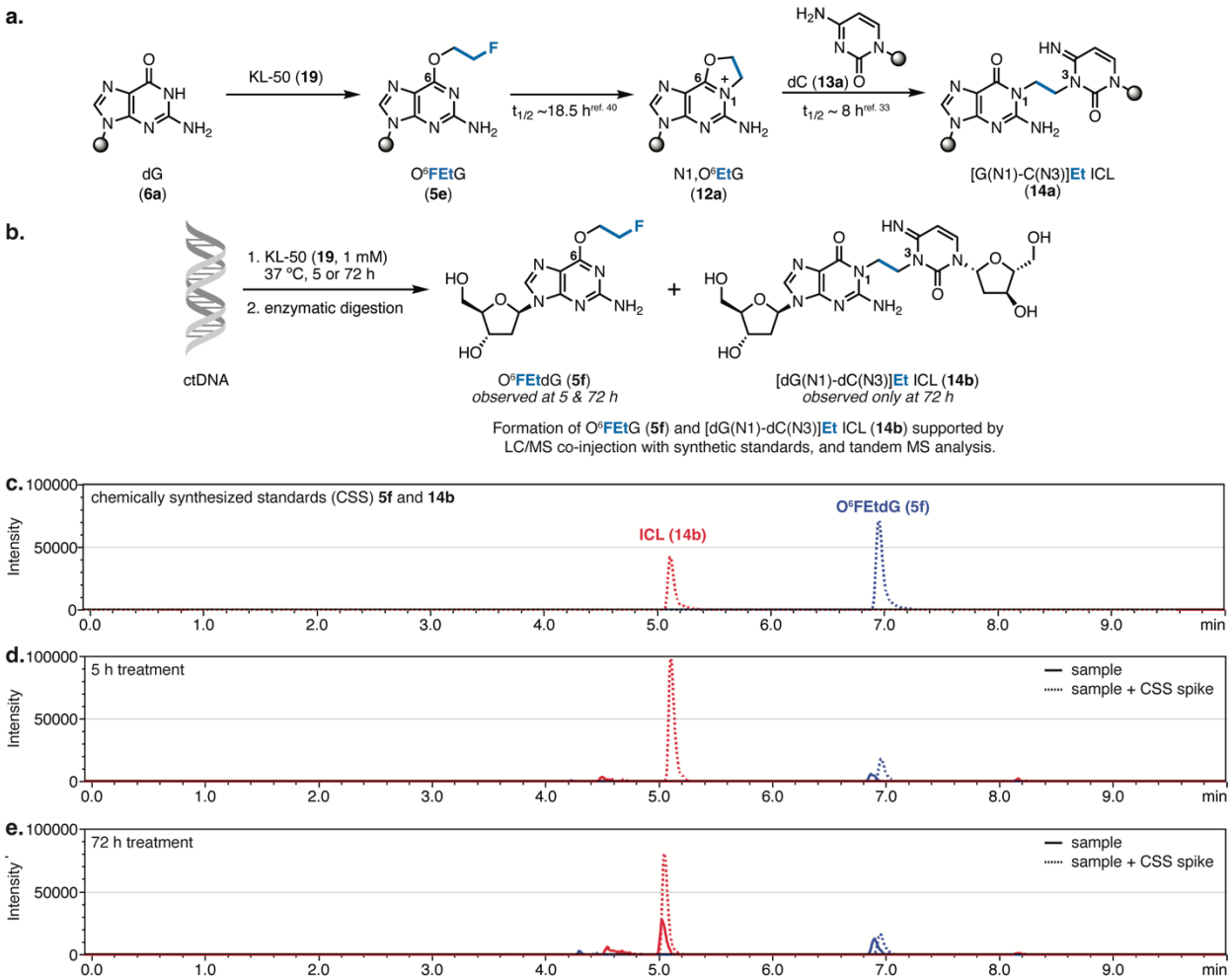

Fig. 9. LC/MS detection of O^{6}FEtdG (**5f**) and the [dG(N])–dC(N3)]Et ICL (**14b**) in calf thymus DNA (ctDNA) treated with KL-50 (**19**) supports formation of DNA ICL **14a** via initial formation of O^{6}FEtG (**5e**). **a.** We hypothesize that treatment of DNA with KL-50 (**19**) leads to initial formation of O^{6}FEtG (**5e**) lesions that evolve to the [G(N1)–C(N3)]Et ICL (**14a**) via N1,O^{6}EtG (**12a**). Under physiological conditions, the half-lives for the transformations **5e→12a** and **12a→14a** are 18.5 and 8 h, respectively. **b.** ctDNA was incubated with KL-50 (**19**, 1 mM) or vehicle at 37 ºC for either 5 or 72 h. Following enzymatic digestion, the resulting nucleoside pools were analyzed by LC/MS/MS. O^{6}FEtdG (**5f**) was observed at 5 and 72 h while the [dG(N1)–dC(N3)]Et ICL (**14b**) was only observed at 72 h. **c.** Extracted ion chromatograms (EICs) for synthetic standards of O^{6}FEtdG (**5f**) and the [dG(N1)–dC(N3)]Et ICL (**14b**). **d–e.** Overlays of EICs for O^{6}FEtdG (**5f**) and the [dG(N])–dC(N3)]Et ICL (**14b**) in the nucleoside pool from ctDNA treated with KL-50 (**19**) for 5 h (panel **d**) or 72 h (panel **e**) before (solid series) and after (dashed series) spiking the LC/MS sample with synthetic standards. For **c**–**e**, positive mode EICs for the calculated *m/z* of the $[M+H]^+$ ion ± 20 ppm were plotted for each species; the intensity of each EIC is given in arbitrary units and was scaled by a factor of 1, 3, and 3 for the EICs in panels **c**, **d**, and **e**, respectively. All data were acquired on LC/MS #1. See Figs. S10–S15 for control experiments and LC/MS/MS data.

Having validated that KL-50 (**19**) forms O^{6}FEtG (**5e**) and the [G(N1)–C(N3)]Et ICL (**14a**) in DNA, we proceeded to compare the rates of DNA ICL formation for O^{6}ClEtG (**5b**) and O^{6}FEtG (**5e**). In a modified alkaline comet assay time-course (t = 2, 8, 24 h), we previously demonstrated that MTZ (**11**, 200 μM) treatment induces ICL formation within 2 h and maximum crosslinking within 8 h in LN229 MGMT–/MMR– cells.[24] In contrast, DNA crosslinking is only observed after 8 h in cells treated with KL-50 (**19**, 200 μM). To study the kinetics of crosslinking in more detail and set the stage to probe DNA–MGMT crosslinking, we targeted the synthesis of a well-defined deoxyoligonucleotide duplex containing a single O^{6}ClEtG (**5b**) or O^{6}FEtG (**5e**) residue. While formation of these O^{6}ClEtG (**5b**)- and O^{6}FEtG (**5e**)-containing duplexes from a common, activated oligonucleotide

duplex precursor was attractive,[53] the instability of O^6ClEtG (**5b**) and O^6FEtG (**5e**) toward N1,O^6EtdG (**12a**) formation (see Fig. 2b) necessitated the synthesis of each duplex from the corresponding phosphoramidite building block in a protected form. Luedtke and coworkers previously disclosed the use of the photolabile N^2-(2-nitrobenzyloxy carbonyl) (NBOC) protecting group to cage O^6ClEtG (**5b**) and studied its DNA crosslinking after photodeprotection (however, this study did not assess the rate of crosslinking).[54] We envisioned that this photodeprotection approach would provide a defined t_0 for our kinetic studies.

The synthesis of the requisite phosphoramidite building blocks **25a** and **25b** began with two-fold protection of commercially available 2′-deoxyguanosine (*tert*-butyldimethylsilyl (TBSCl), imidazole) to provide the bis(*tert*-butyldimethylsilyl) ether **20**, as previously described (Fig. 10).[55] Stepwise NBOC protection of the exocyclic N^2 amine (sodium hydride, 2-nitrobenzyloxy carbonyl imidazole (NBOC-Im)) and O^6-sulfonylation (2,4,6-triisopropylbenzenesulfonyl chloride ($ArSO_2Cl$), triethylamine, 4-(dimethylamino)pyridine (DMAP)),[54] provided the sulfonate **21** (82%, two steps). Treatment of **21** with 1,4-diazabicyclo[2.2.2]octane (DABCO) in tetrahydrofuran generated a quaternary ammonium salt (LC/MS analysis, not shown) that underwent nucleophilic aromatic substitution (S_NAr) upon addition of the corresponding 2-haloethanol and 1,8-diazabicyclo[5.4.0]undec-7-ene (DBU),[56] to yield the O^6-alkylguanosine derivatives **22a** and **22b** (70% and 84%, respectively). Silyl ether cleavage (HF•pyridine)[57] provided the diols **23a** and **23b** (88% and 96%, respectively). Selective protection of the 5′ hydroxyl group (4,4′-dimethoxytrityl chloride (DMTr-Cl), pyridine) then formed the dimethoxytrityl ethers **24a** and **24b** (75% and 65%, respectively). Treatment with 2-cyanoethyl-*N*,*N*,*N*′,*N*′-tetraisopropyl-phosphorodiamidite and 1*H*-tetrazole[58] then provided the phosphoramidites **25a** and **25b**. The purities of **25a** and **25b** were established by quantitative $^{31}P\{^1H\}$ NMR analysis (**25a**: 44% yield, 67 wt% purity; **25b**: 46% yield, 69 wt% purity).

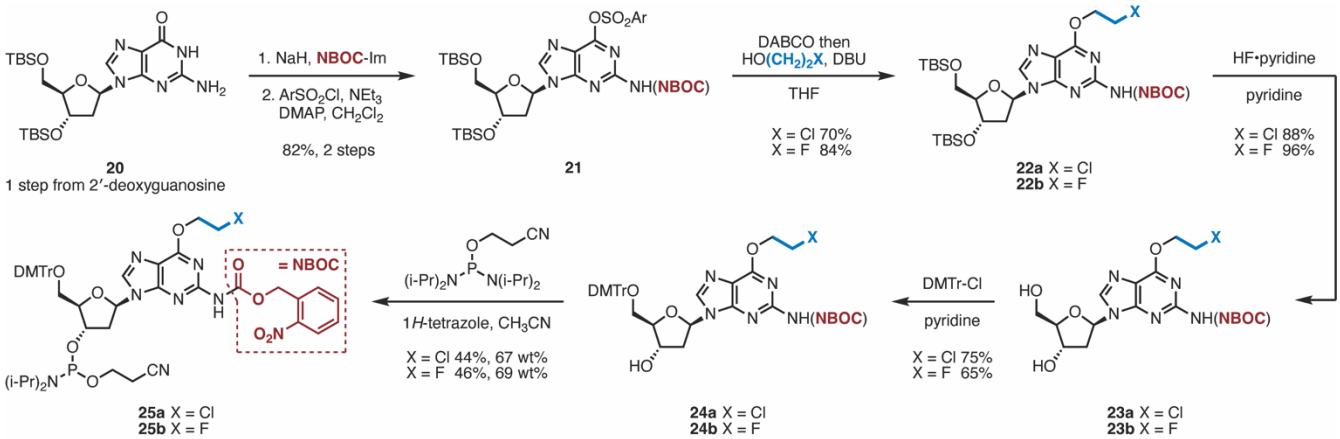

Fig. 10. Synthesis of the photocaged phosphoramidites **25a** and **25b**. Ar = 2,4,6-triisopropylbenzyl.

Solid phase oligonucleotide synthesis using the photocaged phosphoramidites **25a** and **25b** as well as commercially available N^2-phenoxyacetyl-2′-deoxyadenosine, unmodified N^2-isopropyl-phenoxyacetyl-2′-deoxyguanosine, and 2′-deoxythymidine phosphoramidites[54, 59] provided the photocaged oligonucleotides **26a** and **26b**, respectively (Fig. 11a). ^{32}P-5′-End labeling of **26a** and **26b** followed by hybridization to a complementary oligonucleotide generated the deoxyoligonucleotide duplexes **27a** and **27b**, respectively. Notably, the use of a hydroquinone-*O*,*O*′-diacetic acid linker ('Q-linker')[60] that enabled deprotection using diisopropylamine in methanol proved critical as attempts to free the oligonucleotides **26a** and **26b** from resins bearing the more common succinyl linker using this mixture resulted in low conversion, while use of potassium carbonate in methanol provided mixtures of oligonucleotides containing varying amounts of side products arising from cleavage of the NBOC protecting group and/or intramolecular halide displacement (see Figs. S16–S19).

To carry out the crosslinking experiments, each deoxyoligonucleotide duplex was separately irradiated (368 nm LED, 5 min; see Fig. S20 for optimization of irradiation time and Fig. S21 for a visual depiction of the photoirradiation setup), and then incubated at pH 7.2 (20 mM sodium phosphate, 250 mM sodium chloride) at 37 ºC (Fig. 11a). Aliquots were removed starting at t = 0 and immediately diluted with denaturing formamide buffer to arrest crosslinking. Upon completion of the study, the samples were resolved by denaturing polyacrylamide gel electrophoresis (dPAGE, 18%; Fig. 11b and 11d, left-hand lanes). For both duplexes, we observed the time-dependent appearance of crosslinked DNA (**14c**) as a band with lower mobility relative to the single-stranded

oligonucleotide.[54] As expected, the O^6ClEtG containing deoxyoligonucleotide duplex **27a** formed DNA ICLs more rapidly than the O^6FEtG containing duplex **27b**. Quantification of the bands by autoradiography established that the O^6ClEtG containing duplex **27a** transformed to the [G(N1)-C(N3)]Et ICL **14c** with a half-life (relative to the maximum amount of crosslinking) of 6.3 (± 0.04) h (Fig. 11c) while crosslinking by the O^6FEtG containing duplex **27b** was >10-fold slower (half-life = 80 (± 4) h; Fig. 11e). To verify the identity of the ICL (**14c**), we performed a preparative-scale (101 nmol) crosslinking experiment using unlabeled O^6ClEtG containing duplex **27a′** (Fig. S22). Irradiation, incubation (70 h), purification of the ICL by dPAGE, and enzymatic digestion yielded a mixture of unmodified nucleosides and the [dG(N1)-dC(N3)]Et ICL **14b** (Fig. S22a). HPLC co-injection with the synthetic standard as well as tandem mass spectrometry confirmed the formation of the [dG(N1)-dC(N3)]Et ICL **14b** (Fig. S22b–e). We applied transition state theory and carried out transition state search and intrinsic reaction coordinate analysis at the density functional level (DFT)[61] to determine the activation energy for cyclization of O^6-(2-chloroethyl)-N9-methylguanine (**5g**) to N9-methylethanoguanine (**12c**) and O^6-(2-fluoroethyl)-N9-methylguanine (**5h**) to N9-methylethanoguanine (**12c**) in water (Fig. S23). Consistent with intuition and our experimental findings, we found that the activation energy for cyclization of O^6-(2-fluoroethyl)-N9-methylguanine (**5h**) is significantly higher than O^6-(2-chloroethyl)-N9-methylguanine (**5g**; 23.3 and 17.8 kcal/mol, respectively).

As is evident in Figs. 12b and 12d, a large number of bands with decreased mobility compared to the crosslink product **14c** were observed by autoradiography. As these bands were observed at t = 0 min with an intensity that did not increase with time, we speculated that they may be the result of non-selective, irradiation induced crosslinking. However, irradiation of the corresponding duplex containing an unmodified guanine residue (**27c,** Fig. S24a and c) did not give rise to these bands, indicating they did not arise from UV-mediated damage to the DNA. As such, we hypothesized that these bands derived from non-specific side reactions of the DNA with the reactive nitrosoarene formed on photodeprotection.[62] To test this hypothesis, we synthesized the deoxyoligonucleotide duplexes **27d** and **27e** containing an O^6-methylguanine residue or an N^2-NBOC-O^6-methylguanine residue, respectively, in place of the O^6-(2-haloethyl)guanine residues in **27a** and **27b** (Fig. S24a). The deoxyoligonucleotide duplex **27d** was synthesized from the commercially available O^6-methylguanine phosphoramidite. The NBOC-protected deoxyoligonucleotide duplex **27e** was synthesized from the corresponding N^2-NBOC-O^6-methylguanine phosphoramidite **25d**, which was prepared by a route analogous to that shown in Fig. 10 (Fig. S24b). In support of our hypothesis, a pattern of lower-mobility bands similar to those shown in Figs. 11b and 11d were observed only when the NBOC-protected deoxyoligonucleotide duplex **27e**, but not **27d**, was subjected to photoirradiation and denaturing gel electrophoresis (Fig. S24c).

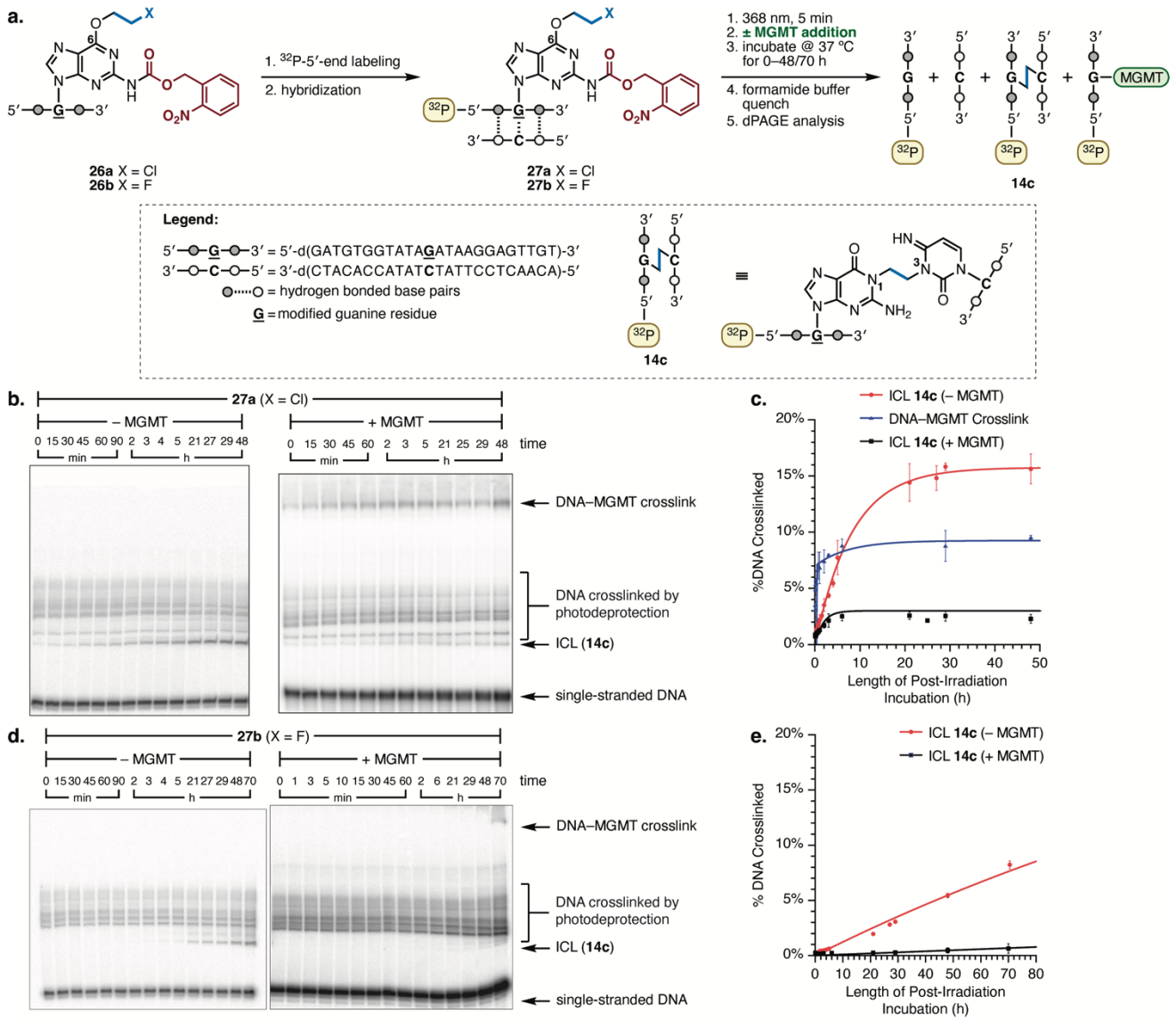

Fig. 11. Kinetic study of ICL **14c** and DNA–MGMT crosslink formation using the O^{6}XEtG containing deoxyoligonucleotide duplexes **27a** (X = Cl) and **27b** (X = F) in the absence and presence of MGMT. **a.** Experimental design. **b.** Representative denaturing gel for the kinetic study of the O^{6}ClEtG-containing duplex **27a** ± 5 equivalents of human MGMT. **c.** Plot of %DNA crosslinked versus time as quantified by autoradiography for the kinetic study of O^{6}ClEtG containing duplex **27a**. **d.** Representative denaturing gel of the kinetic study of the O^{6}FEtG containing duplex **27b** ± 5 equivalents of human MGMT. **e.** Plot of %DNA crosslinked versus time as quantified by autoradiography for the kinetic study of O^{6}FEtG containing duplex **27b**. For **c** and **e**, points indicate mean; error bars indicate standard deviation; n = 3 biological replicates.

The DNA crosslinking studies presented above establishe that the O^{6}FEtG lesion (**5e**) derived from KL-50 (**19**) generates DNA ICLs more slowly than the O^{6}ClEtG lesion (**5b**) derived from MTZ (**11**) or lomustine (**10**). Because this crosslinking mechanism proceeds through the common intermediate N1,O^{6}EtG (**12a**), the difference in observed rates of DNA ICL formation must derive from the slower rate of cyclization of O^{6}FEtG (**5e**) to N1,O^{6}EtG (**12a**), relative to O^{6}ClEtG (**5b**). A central element of our mechanistic analysis (see Fig. 2 and associated text) is that the slower rate of cyclization of O^{6}FEtG (**5e**) to N1,O^{6}EtG (**12a**) will provide more time for MGMT to reverse O^{6}FEtG (**5e**) in healthy tissue, thereby reducing the amount of toxic DNA–MGMT crosslinks derived from the reaction of N1,O^{6}EtG (**12a**) with MGMT. We reasoned that addition of MGMT to solutions of the O^{6}XEtG containing deoxyoligonucleotide duplexes **27a** (X = Cl) and **27b** (X = F) immediately after photodeprotection would allow us to test this hypothesis. Additionally, this assay would also enable us to directly assess the degree to which MGMT can prevent DNA ICL formation from **27a** and **27b**.

We found that DNA ICL production was reduced but not completely ablated when the O^6ClEtG containing duplex **27a** was exposed to MGMT (5.0 equiv) immediately following photodeprotection (Fig. 11b, right-hand lanes). A plot of %DNA crosslinked as a function of time revealed a ~2-fold reduction in the formation of DNA ICL **14c** after 2 h (Fig. 11c). A band of low mobility, consistent with a DNA–MGMT crosslink, was observed at the top of the gel immediately after addition of MGMT. This nearly instantaneous formation of DNA–MGMT crosslinks is consistent with rapid formation of N1,O^6EtG (**12a**) following photodeprotection of the O^6ClEtG containing duplex **27a** (Fig. 11c; see also Fig. S25c, vida infra). By comparison, we found that production of the DNA ICL **14c** was almost completely ablated when the O^6FEtG containing duplex **27b** was exposed to MGMT (5.0 equiv) immediately following photodeprotection (Fig. 11d, right-hand lanes). A plot of %DNA crosslinked as a function of time reveals that the addition of MGMT reduced of DNA-crosslinking ~8 fold at 70 h (Fig. 11e). We detected trace amounts of MGMT–DNA cross-links at later time points in the assay (48–70 h).

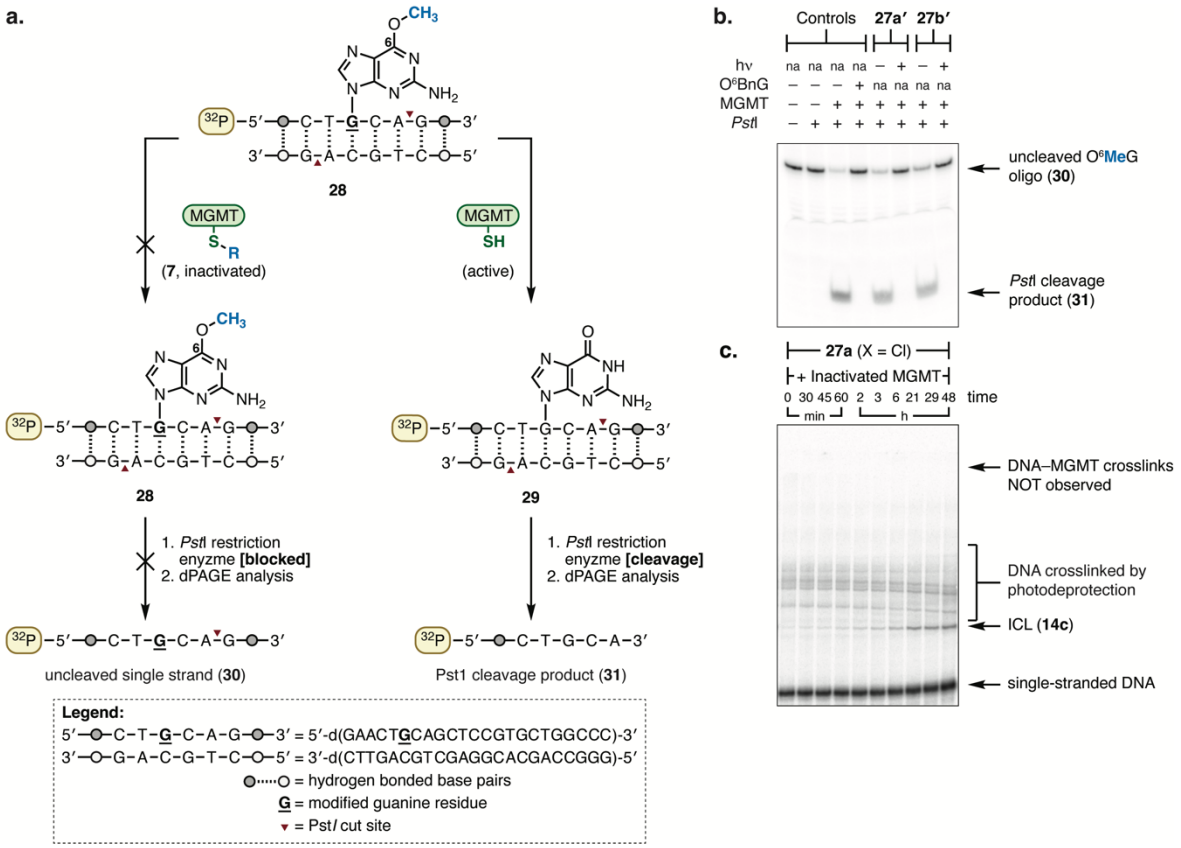

Fig. 12. MGMT's active cite cysteine residue (Cys145) is involved in the formation of DNA–MGMT crosslinks and in preventing formation of the DNA ICL **14c**. **a.** Schematic of the *Pst*I restriction enzyme-based MGMT activity assay that leverages the inability of the restriction enzyme *Pst*I to cleave DNA if its restriction site contains an O^6MeG residue. If the 5′-^{32}P labeled, O^6MeG containing duplex **28** is treated with MGMT (**7**) inactivated by the alkylation of its active site cysteine (Cys145), the O^6MeG lesion is not repaired and the uncleaved single strand **30** is observed by dPAGE analysis (panel **a**–left). Subsequent treatment of the unrepaired duplex **28** with the *Pst*I restriction enzyme does not result in strand cleavage. If the O^6MeG containing duplex **28** is treated with active MGMT, the O^6MeG lesion is repaired to give repaired duplex **29** (panel **a**–right). Subsequent treatment of **29** with the *Pst*I restriction enzyme results in strand cleavage to produce an 8-mer cleavage product **31** upon dPAGE analysis. **b.** Unlabeled duplexes **27a′** and **27b′** were irradiated (368 nm) then incubated with human MGMT at 3 h at 37 ºC, allowing for inactivation of MGMT by transfer of the O^6XEtG lesion to the protein's active site cysteine. As such, upon addition of O^6MeG containing duplex **28**, the O^6MeG lesion is not repaired and subsequent addition of *Pst*I does not the produce cleavage product (as in panel **a**-left). In contrast, repetition of the experiment with non-irradiated duplexes **27a′** and **27b′** produces the cleavage product **31**, indicating that MGMT was not able to repair the O^6XEtG lesion in the presence of the N2-NBOC protecting group (as in panel **a**-right). Control experiments show that the cleavage product **31** is only observed when the O^6MeG containing duplex **28** is treated with MGMT prior to the introduction of *Pst*I and that inactivation of MGMT via pretreatment with O^6BnG (20 equiv, 1 h) prevents repair of the O^6MeG lesion upon addition of the labeled O^6MeG containing duplex **28**, leading to an absence of the cleavage product upon introduction of *Pst*I. **c.** Addition of MGMT inactivated via pre-treatment with O^6BnG (20 equiv, 1 h) to irradiated O^6ClEtG containing duplex **27a** does not result in the formation DNA–MGMT crosslink and results in the formation of the ICL **14c** at nearly the same level as observed in the absence of MGMT (see Fig. 11b, left-hand lanes). For **a**, only the 5′-^{32}P-labeled products of each reaction are drawn. For **b**, duplexes **27a′** and **27b′** are identical in structure to duplexes **27a** or **27b**, respectively (Fig. 11a), except that **27a′** and **27b′** lack the 5′-^{32}P label.

To verify that MGMT decreased the formation of DNA ICL **14c** and caused the formation of DNA–MGMT crosslinks via the protein's active site cysteine residue (Cys135), we performed two assays. In the first, we used a restriction enzyme based MGMT activity assay[63] to demonstrate that pre-exposure of MGMT to irradiated, unlabeled duplexes **27a′** and **27b′** inhibits the protein's ability to repair a duplex containing a *Pst*I restriction site blocked by an O^6MeG residue (Fig. 12a–b). Notably, this assay also showed that the small amount of DNA–MGMT crosslinks observed for **27b** does not result from insufficient interaction between MGMT and the duplex. In a second assay, we verified that the decrease in ICL formation and formation of DNA–MGMT crosslinks upon addition of MGMT to the O^6ClEtG containing duplex **27a** following photodeprotection specifically involves the protein's active site cysteine residue (Cys145). We inactivated MGMT by treatment for 1 h with the known MGMT substrate O^6-benzylguanine (O^6BnG)[64] then added this deactivated MGMT to photodeprotected duplex **27a**. We found that addition of O^6BnG treated MGMT resulted in no MGMT–DNA crosslink formation and an increase in amount of DNA ICLs **14c** to nearly the same level as observed in the absence of MGMT (Fig. 12c).

It is important to note that, due to the short half-life for cyclization of O^6ClEtG (**5b**) to the N1,O^6EtG (**12a**, $t_{1/2}$ = ~ 18 min for the isolated nucleoside **5d**,[38] Fig. 2b) the 5 min duration of the photodeprotection prior to the introduction of MGMT may allow O^6ClEtG (**5b**) lesions that would have been repaired by MGMT to instead evolve to N1,O^6EtG (**12a**) in the protein's absence. This would artificially increase the amount of DNA–MGMT crosslinks observed as, under physiological conditions, ring-opening of N1,O^6EtG (**12a**) to the ICL **14a** is comparatively slow ($t_{1/2}$ ~ 8 h,[33] Fig. 2b), and MGMT is present before introduction of the DNA alkylation agent. This issue has been noted in earlier studies of DNA–MGMT crosslinks.[32a, 32c] To address this, we carried out an experiment wherein MGMT was added immediately before irradiation (Fig. S25). While it is theoretically possible that MGMT may reverse the O^6ClEtG in **27a** before photodeprotection, we found that non-irradiated duplex **27a** did not deactivate MGMT (Fig. 12a). To control for potential light-mediated degradation of MGMT, we conducted a control experiment wherein the O^6ClEtG containing duplex **27a** and MGMT were irradiated separately and then combined prior to incubation. We found that the levels of ICL **14c** formation (Fig. S25a) and MGMT–DNA crosslinking (Fig. S25b) were not measurably altered by the addition of MGMT to the O^6ClEtG containing duplex **27a** before or after irradiation. Furthermore, we found little difference between the results from post-irradiation addition of non-irradiated and irradiated MGMT, indicated that the irradiation does not affect MGMT's activity. As such, the 5 min delay between the start of photodeprotection and the addition of MGMT does not artificially increase the amount of DNA–MGMT crosslinks. This indicates that the experiments described above with the O^6ClEtG containing duplex **27a** in the absence and presence of MGMT provide a good model for the physiological treatment of MGMT– and MGMT+ cells, respectively, with 2-chloroethylating agents. We regard the experiments described above with the O^6FEtG containing duplex **27a** as even more robust owing to the slower rate of conversion of O^6FEtG (**5e**) to N1,O^6EtG (**12a**) ($t_{1/2}$ ~ 18.5 h for the isolated nucleoside **5c**[40], Fig. 3).

Conclusion.

The standard of care for newly-diagnosed GBM has not changed since Stupp's landmark 2005 clinical trial established that adjuvant treatment with TMZ (**1**) provides a ~7 month survival benefit for GBM patients newly-diagnosed with tumors deficient in the DNA repair protein MGMT.[2,3] The ubiquity of MGMT expression in heathy tissues provides a therapeutic index between healthy and cancerous cells. However, ~50% of these MGMT– tumors will become resistant to TMZ (**1**) by a loss of MMR activity.[19] Though this resistance mechanism was first elucidated in colorectal cancer in 1995,[19c] no progress has been recorded in developing agents that overcome MMR-based resistance while retaining selectivity for MGMT– cell lines. Lomustine (**10**), a DNA ICL forming alkylator commonly given to recurrent GBM patients, is impervious to MMR resistance[24] but lacks selectivity for MGMT– cells (see Fig. 5c) and provides only a marginal survival benefit in the clinic.[20] Similarly, MTZ (**10**), a DNA ICL forming derivative of TMZ (**1**), overcomes MMR-related resistance[24] at the expense of selectivity for MGMT– cells (see Fig. 5d) and was abandoned in clinical trials due to toxicity.[26]

Our work was motivated by literature reports suggesting that the toxicity of lomustine (**10**) and MTZ (**11**) in MGMT+ cells is not driven by DNA ICL formation,[27a, 28] but rather by the formation of DNA–MGMT crosslinks.[32-33] Chemical rate data suggest that N1,O^6EtG (**12a**), the electrophilic intermediate intercepted by MGMT to form DNA–MGMT crosslinks, accumulates in MGMT+ cells treated with lomustine (**10**) and MTZ (**11**) due to rapid cyclization of the initially formed O^6ClEtG (**5b**) lesion (Fig. 2).[33, 37-38] We hypothesized that a crosslinking agent capable of generating an O^6G lesion that cyclized more slowly to N1,O^6EtG (**12a**), but which was still readily

reversed by MGMT, might decrease the amount of DNA–MGMT crosslinks formed in healthy (MGMT+) tissues while maintaining potency against MMR– cells and, ultimately, lead to an agent effective against recurrent, MGMT–/MMR– GBM.

Our long-term clonogenic survival assays demonstrate that KL-50 (**19**) is potent against MMR+ and MMR– cells while maintaining high selectivity for MGMT– cells (Fig. 5). A PRISM multiplexed viability screen of KL-50 (**19**) using 902 well-characterized cancer cell lines showed that *MGMT* expression is the single most important determinant of KL-50 (**19**) toxicity, further validating our clonogenic survival assays (Fig. 6). Data from a modified alkaline comet assay and denaturing electrophoresis of genomic DNA from KL-50 (**19**)-treated cells shows that KL-50 (**19**) only induces DNA ICLs in MGMT– cell lines (Fig. 8). As we had previously established that the generation of DNA ICLs was central to KL-50 (**19**)'s mode of toxicity,[24] these data provide a strong connection between mechanism of action and MGMT-based selectivity.

We envisioned that KL-50 (**19**) would generate DNA ICLs by a mechanism analogous to that of the DNA ICL forming 2-chloroethylating agents such as lomustine (**10**).[22, 65] Specifically, we hypothesized that alkylation of DNA by KL-50 (**19**) would lead to initial formation of an O^6FEtG lesion (**5e**) that would develop into an electrophilic N1,O^6EtG intermediate (**12a**) that would evolve into the [G(N1)–C(N3)]Et ICL (**14a**) upon nucleophilic capture by the based paired cytidine residue (**13a**; Fig 9a). Observation of the corresponding nucleosides O^6FEtdG (**5f**) and [dG(N1)–dC(N3)]Et ICL (**14b**) by LC/MS in nucleoside pools obtained from enzymatic digestion of calf thymus DNA treated with KL-50 (**19**, Fig. 9b–d) lends support to this mechanism of action. Studies using chemically defined, photocaged deoxyoligonucleotides[54] allowed us to study the kinetics of this ICL formation in detail. We found that, upon photodeprotection, the O^6XEtG containing duplexes **27a** (X = Cl) and **27b** (X = F) generated the DNA ICL **14c** at rates differing by >10 fold (**27a**, $t_{1/2}$ = 6.3 ± 0.04 h; **27b**, $t_{1/2}$ = 80 ± 4 h; Fig. 11). As the O^6XEtG lesions **5b** (X = Cl) and **5e** (X = F) yield the [G(N1)–C(N3)]Et ICL **14a** via halide displacement to give the common, cyclized intermediate N1,O^6EtG (**12a**, see Fig. 2b and 9a), this indicates that the difference in rates observed in the deoxynucleotide experiments is the result of slower cyclization for X = F as compared to X = Cl, as would be expected based on the poor leaving group ability of fluoride. This is consistent with previously described model studies on the rates of hydrolysis for O^6-(2-fluoroethyl)guanosine (**5c**, $t_{1/2}$ ~ 18.5 h)[40] and O^6-(2-chloroethyl)guanosine (**5d**, $t_{1/2}$ ~ 18 min; Fig. 3)[38] as well as our DFT studies comparing the activation energies for the cyclization of O^6-(2-fluoroethyl)-N9-methylguanine (**5h**; ΔG_a = 23.3 kcal/mol) and O^6-(2-chloroethyl)-N9-methylguanine (**5g**; ΔG_a 17.8 kcal/mol) to the common intermediate N9-methylethanoguanine (**12c**; Fig. S23).

Our data suggest that the persistence of O^6FEtG (**5e**) provides more time for MGMT to reverse the initial alkylation in healthy cells. This is supported by our deoxyoligonucleotide duplex studies which established that addition of MGMT immediately after photodeprotection nearly eliminates DNA ICL formation from the O^6FEtG containing duplex **27b** (Fig. 11d, right-hand lanes), while MGMT was less effective in preventing ICL formation from the O^6ClEtG containing duplex **27a** (Fig. 11b, right-hand lanes). Significantly, the slower rate of conversion of O^6FEtG (**5e**) to N1,O^6EtG (**12a**) minimizes the accumulation of the latter in MGMT+ cells. Prior studies established that ring-opening of N1,O^6EtG (**12a**) leads to MGMT–DNA crosslinks.[33] Consistent with this, we found MGMT–DNA crosslinks are much more abundant when the O^6ClEtG containing duplex **27a** was exposed to MGMT following photodeprotection, relative to the O^6FEtG containing duplex **27b** (Figs. 12b,d, right-hand lanes). Finally, consistent with this higher selectivity, KL-50 (**19**) demonstrated efficacy and tolerability in a PDX model of MGMT–/MMR– GBM, while lomustine (**10**) was ineffective (Fig. 7).

As presented in Fig. 2b, there are at least two mechanisms by which MGMT–DNA crosslinks may form. We believe the formation of small amounts of MGMT–DNA crosslinks at later time points in experiments employing the O^6FEtG-containing duplex **27b** is more consistent with their formation by ring-opening of N1,O^6EtG (**12a**) rather than through the episulfonium intermediate **15**. We base this on two observations. First, Guengerich and co-workers demonstrated that the half-life for the hydrolysis of *S*-(2-fluoroethyl)glutathione is 37 min (22 ºC, pH 7.4).[66] As this hydrolysis proceeds through an episulfonium intermediate that can form DNA adducts,[67] we would expect to see MGMT–DNA crosslinks derived from episulfonium ion opening at earlier time points in our study if this mechanism were operative, as our data indicate that the repair of O^6FEtG (**5e**) by MGMT, which would generate the episulfonium precursor, is faster than evolution of O^6FEtG (**5e**) to N1,O^6EtG (**12a**). Second, we did not observe DNA–MGMT crosslinks using duplex **27b** in the absence of the reducing agent dithiothreitol (DTT). DTT is necessary to maintain the MGMT's active site cysteine residue in its reduced form during the 48 h incubation period

of the experiment. The formation of DPCs via an episulfonium ion pathway would be expected to have less dependence on DTT due to the more rapid rate of O^6FEtG (**5e**) repair by MGMT as compared to N1,O^6EtG (**12a**) formation.

It is important to note that MGMT activity has also been characterized as a mechanism of resistance to DNA alkylating agents, including TMZ (**1**),[68] and efforts to develop "MGMT–independent" therapeutics have been recorded. For example, VAL-083 (aka dianhydrogalacitol) is a diepoxide-based DNA crosslinking agent that is being evaluated in clinical trials of MGMT+ GBM, with the goal of overcoming MGMT-based resistance to TMZ (**1**).[69] Additionally, TMZ derivatives that exert toxicity independent of MGMT status have been described.[70] The notion that MGMT-silencing might provide a therapeutic index (TI) when alkylation agents are administered systemically to patients harboring MGMT– tumors was first recognized in 1980.[71] Our own opinion is that it will be difficult to achieve efficacious level of exposure to systematically-administered DNA alkylation agents without a mechanism, such as MGMT silencing, to obtain selective tumor toxicity. While our work is unlikely to benefit patients with MGMT+ tumors, it may provide a treatment option for recurrent, TMZ-resistant, MGMT– GBM. Additionally, the comparable activity of KL-50 (**19**) to TMZ (**1**) in MGMT–/MMR+ models of GBM suggests its potential use in the up-front setting.

ASSOCIATED CONTENT

The Supporting Information contains supplementary figures and tables, detailed experimental procedures, and characterization data for all new compounds.

AUTHOR INFORMATION

Corresponding Authors

Ranjit S. Bindra – *Departments of Pathology and Therapeutic Radiology, Yale School of Medicine, New Haven, Connecticut 06520, United States;* orcid.org/0000-0002-3255-0467; Email: ranjit.bindra@yale.edu

Seth B. Herzon – *Department of Chemistry, Yale University, New Haven, Connecticut 06520, United States; Departments of Pharmacology and Therapeutic Radiology, Yale School of Medicine, New Haven, Connecticut 06520, United States;* orcid.org/0000-0001-5940-9853; Email: seth.herzon@ yale.edu

Authors

Eric D. Huseman – *Department of Chemistry, Yale University, New Haven, Connecticut 06520, United States;* orcid.org/0000-0002-7550-1593.

Anna Lo – *Department of Chemistry, Yale University, New Haven, Connecticut 06520, United States;* orcid.org/0000-0002-4489-3109.

Olga Fedorova – *Department of Molecular, Cellular, and Developmental Biology, Yale University, New Haven, Connecticut 06520, United States; Howard Hughes Medical Institute, Yale University, New Haven, Connecticut 06520, United States;* orcid.org/0000-0001-5995-7358.

James L. Elia – *Department of Pathology, Yale School of Medicine, New Haven, Connecticut 06520, United States;* orcid.org/0000-0003-3962-7452.

Susan E. Gueble – *Department of Therapeutic Radiology, Yale School of Medicine, New Haven, Connecticut 06520, United States;* orcid.org/0000-0002-8043-1147.

Kingson Lin – *Department of Chemistry, Yale University, New Haven, Connecticut 06520, United States; Departments of Pathology and Therapetuic Radiology, Yale School of Medicine, New Haven, Connecticut 06520, United States;* orcid.org/0000-0002-5460-4008.

Ranjini Sundaram – *Department of Therapeutic Radiology, Yale School of Medicine, New Haven, Connecticut 06520, United States;* orcid.org/0000-0002-5725-0284.

Danielle M. Burgenske – *Department of Radiation Oncology, Mayo Clinic, Rochester, Minnesota;* orcid.org/0000-0003-0014-5579.

Joonseok Oh – *Department of Chemistry, Yale University, New Haven, Connecticut 06520, United States; Institute of Biomolecular Design & Discovery, Yale University; West Haven, CT, United States*.

Jinchan Liu – *Department of Chemistry, Yale University, New Haven, Connecticut 06520, United States;* orcid.org/ 0000-0003-2217-1233.

Fabian Menges – *Department of Chemistry, Yale University, New Haven, Connecticut 06520, United States; Department of Chemistry, Chemical and Biophysical Instrumentation Center, Yale University, New Haven, Connecticut 06520, United States;* orcid.org/0000-0002-5859-9197.

Matthew G. Rees – *Broad Institute of MIT and Harvard, Cambridge, Massachusetts 02142, Unites States;* orcid.org/0000-0002-2987-7581.

Melissa M. Ronan – *Broad Institute of MIT and Harvard, Cambridge, Massachusetts 02142, Unites States;* orcid.org/0000-0003-4269-1404.

Jennifer A. Roth – *Broad Institute of MIT and Harvard, Cambridge, Massachusetts 02142, Unites States;* orcid.org/0000-0002-5117-5586.

Victor S. Batista – *Department of Chemistry, Yale University, New Haven, Connecticut 06520, United States;* orcid.org/0000-0002-3262-1237.

Jason M. Crawford – *Department of Chemistry, Yale University, New Haven, Connecticut 06520, United States; Institute of Biomolecular Design & Discovery, Yale University; West Haven, CT, United States; Department of Microbial Pathogenesis, Yale School of Medicine; New Haven, Connecticut, United States;* orcid.org/0000-0002-7583-1242.

Jann N. Sarkaria – *Department of Radiation Oncology, Mayo Clinic, Rochester, Minnesota;* orcid.org/0000-0001-7489-4885.

Anna M. Pyle – *Departments of Chemistry and Molecular, Cellular, and Developmental Biology, Yale University, New Haven, Connecticut 06520, United States; Howard Hughes Medical Institute, Yale University, New Haven, Connecticut 06520, United States;* orcid.org/0000-0001-9045-8872.

Notes

The authors declare the following competing interests: S.B.H., R.S.B., and K.L. are cofounders and hold equity in Modifi Biosciences, which has exclusive rights to the findings herein. S.B.H. and R.S.B. are officers of Modifi Biosciences. J.N.S. is a member of the Scientific Board of Directors of Modifi Biosciences. E.D.H. was a consultant for Modifi Biosciences. K.L., S.E.G., R.K.S., E.D.H., R.S.B., and S.B.H. are inventors on US Provisional Application 63/290,572 submitted by Yale University, which covers the mechanism of action and use of KL-50 (**19**) for the treatment of MGMT–/ MMR– GBM. K.L., R.S.B., and S.B.H. are inventors on US Provisional Applications 63/209,763, 63/212,410, 63/247,645, 63/290,622, 63/290,627, and 63/290,630, which cover KL-50 (**19**) and related derivatives for the treatment of MGMT– tumors.

ACKNOWLEDGMENTS

Financial support from Modifi Biosciences, the NIH-NIGMS (R35-GM131913 to S.B.H.), the NIH-NCI (U19CA264362 to R.S.B.), and the Yale Cancer Center (Pilot Grant to S.B.H. and R.S.B.) is gratefully acknowledged. Purification and NMR characterization of the [dG(N1)–dC(N3)]Et ICL (**14b**) was supported by the DOD (W81XWH2110547). This research made use of the Chemical and Biophysical Instrumentation Center at Yale University (RRID:SCR_021738). Equipment was purchased with funds from Yale University. Dr. Jonathan Ellefsen is acknowledged for assembling the photoreactor. S.B.H. dedicates this paper to the memory of Mr. William McKale.

REFERENCES

(1) (a) Oronsky, B.; Reid, T. R.; Oronsky, A.; Sandhu, N.; Knox, S. J. A Review of Newly Diagnosed Glioblastoma. *Front. Oncol.* **2020,** *10*, 574012. (b) Lin, D.; Wang, M.; Chen, Y.; Gong, J.; Chen, L.; Shi, X.; Lan, F.; Chen, Z.; Xiong, T.; Sun, H.; Wan, S. Trends in Intracranial Glioma Incidence and Mortality in the United States, 1975-2018. *Front. Oncol.* **2021,** *11*, 748061.

(2) Stupp, R.; Mason, W. P.; van den Bent, M. J.; Weller, M.; Fisher, B.; Taphoorn, M. J.; Belanger, K.; Brandes, A. A.; Marosi, C.; Bogdahn, U.; Curschmann, J.; Janzer, R. C.; Ludwin, S. K.; Gorlia, T.; Allgeier, A.; Lacombe, D.; Cairncross, J. G.; Eisenhauer, E.; Mirimanoff, R. O.; European Organisation for, R.; Treatment of Cancer Brain, T.; Radiotherapy, G.; National Cancer Institute of Canada Clinical Trials, G. Radiotherapy Plus Concomitant and Adjuvant Temozolomide for Glioblastoma. *N. Engl. J. Med.* **2005,** *352*, 987–996.

(3) Hegi, M. E.; Diserens, A. C.; Gorlia, T.; Hamou, M. F.; de Tribolet, N.; Weller, M.; Kros, J. M.; Hainfellner, J. A.; Mason, W.; Mariani, L.; Bromberg, J. E.; Hau, P.; Mirimanoff, R. O.; Cairncross, J. G.; Janzer, R. C.; Stupp, R. MGMT Gene Silencing and Benefit from Temozolomide in Glioblastoma. *N. Engl. J. Med.* **2005,** *352*, 997–1003.

(4) Pegg, A. E. Multifaceted Roles of Alkyltransferase and Related Proteins in DNA Repair, DNA Damage, Resistance to Chemotherapy, and Research Tools. *Chem. Res. Toxicol.* **2011,** *24*, 618–639.

(5) Boulden, A. M.; Foote, R. S.; Fleming, G. S.; Mitra, S. Purification and Some Properties of Human DNA-O^6-Methylguanine Methyltransferase. *J. Biosci.* **1987,** *11*, 215–224.

(6) Courtesy of Human Protein Atlas, www.proteinatlas.org ,see: Karlsson Karlsson, M.; Zhang, C.; Méar, L.; Zhong, W.; Digre, A.; Katona, B.; Sjöstedt, E.; Butler, L.; Odeberg, J.; Dusart, P.; Edfors, F.; Oksvold, P.; von Feilitzen, K.; Zwahlen, M.; Arif, M.; Altay, O.; Li, X.; Ozcan, M.; Mardinoglu, A.; Fagerberg, L.; Mulder, J.; Luo, Y.; Ponten, F.; Uhlén, M.; Lindskog, C. A Single–cell Type Transcriptomics Map of Human Tissues. *Sci. Adv.* **2021,** *7*, eabh2169.

(7) Alnahhas, I.; LaHaye, S.; Giglio, P.; Mardis, E.; Puduvalli, V. An Evaluation of MGMT Promoter Methylation within the Methylation Subclasses of Glioblastoma. *Neuro-oncol. Adv.* **2020,** *2*, vdaa117.
(8) Weller, M.; Stupp, R.; Reifenberger, G.; Brandes, A. A.; van den Bent, M. J.; Wick, W.; Hegi, M. E. MGMT Promoter Methylation in Malignant Gliomas: Ready for Personalized Medicine? *Nat. Rev. Neurol.* **2010,** *6*, 39–51.
(9) Shen, L.; Kondo, Y.; Rosner, G. L.; Xiao, L.; Hernandez, N. S.; Vilaythong, J.; Houlihan, P. S.; Krouse, R. S.; Prasad, A. R.; Einspahr, J. G.; Buckmeier, J.; Alberts, D. S.; Hamilton, S. R.; Issa, J. P. MGMT Promoter Methylation and Field Defect in Sporadic Colorectal Cancer. *J. Natl. Cancer Inst.* **2005,** *97*, 1330–1338.
(10) Tuominen, R.; Jewell, R.; van den Oord, J. J.; Wolter, P.; Stierner, U.; Lindholm, C.; Hertzman Johansson, C.; Lindén, D.; Johansson, H.; Frostvik Stolt, M.; Walker, C.; Snowden, H.; Newton-Bishop, J.; Hansson, J.; Egyházi Brage, S. Headline Capitalization/ Title Case Tool. *Int. J. Cancer* **2015,** *136*, 2844–2853.
(11) Gu, C.; Lu, J.; Cui, T.; Lu, C.; Shi, H.; Xu, W.; Yuan, X.; Yang, X.; Huang, Y.; Lu, M. Association between MGMT Promoter Methylation and Non-Small Cell Lung Cancer: A Meta-Analysis. *PLoS One* **2013,** *8*, e72633.
(12) Jakob, J.; Hille, M.; Sauer, C.; Ströbel, P.; Wenz, F.; Hohenberger, P. O6-Methylguanine-DNA Methyltransferase (MGMT) Promoter Methylation Is a Rare Event in Soft Tissue Sarcoma. *Radiat. Oncol.* **2012,** *7*, 180.
(13) Stevens, M. F. G., CHAPTER 7 - Temozolomide: From Cytotoxic to Molecularly-Targeted Agent. In *Cancer Drug Design and Discovery*, Neidle, S., Ed. Academic Press: New York, 2008; pp 157-172.
(14) Denny, B. J.; Wheelhouse, R. T.; Stevens, M. F.; Tsang, L. L.; Slack, J. A. NMR and Molecular Modeling Investigation of the Mechanism of Activation of the Antitumor Drug Temozolomide and Its Interaction with DNA. *Biochem.* **1994,** *33*, 9045–9051.
(15) Wheelhouse, R. T.; Stevens, M. F. G. Decomposition of the Antitumour Drug Temozolomide in Deuteriated Phosphate Buffer: Methyl Group Transfer Is Accompanied by Deuterium Exchange. *J. Chem. Soc., Chem. Commun.* **1993**, 1177–1178.
(16) Bull, V. L. Studies on the Mode of Cytotoxicity of Imidazotetrazines. The University of Aston in Birmingham, 1988.
(17) Zhang, J.; Stevens, M. F.; Bradshaw, T. D. Temozolomide: Mechanisms of Action, Repair and Resistance. *Curr. Mol. Pharmacol.* **2012,** *5*, 102–114.
(18) For a review on futile cycling, see: Li, Z.; Pearlman, A. H.; Hsieh, P. DNA Mismatch Repair and the DNA Damage Response. *DNA Repair* **2016,** *38*, 94–101.
(19) (a) Indraccolo, S.; Lombardi, G.; Fassan, M.; Pasqualini, L.; Giunco, S.; Marcato, R.; Gasparini, A.; Candiotto, C.; Nalio, S.; Fiduccia, P.; Fanelli, G. N.; Pambuku, A.; Della Puppa, A.; D'Avella, D.; Bonaldi, L.; Gardiman, M. P.; Bertorelle, R.; De Rossi, A.; Zagonel, V. Genetic, Epigenetic, and Immunologic Profiling of MMR-Deficient Relapsed Glioblastoma. *Clin. Cancer Res.* **2019,** *25*, 1828–1837. (b) Yu, Y.; Villanueva-Meyer, J.; Grimmer, M. R.; Hilz, S.; Solomon, D. A.; Choi, S.; Wahl, M.; Mazor, T.; Hong, C.; Shai, A.; Phillips, J. J.; Wainer, B. H.; McDermott, M.; Haas-Kogan, D.; Taylor, J. W.; Butowski, N.; Clarke, J. L.; Berger, M. S.; Molinaro, A. M.; Chang, S. M.; Costello, J. F.; Oberheim Bush, N. A. Temozolomide-Induced Hypermutation Is Associated with Distant Recurrence and Reduced Survival after High-Grade Transformation of Low-Grade IDH-Mutant Gliomas. *Neuro-Oncol.* **2021,** *23*, 1872–1884. (c) Branch, P.; Hampson, R.; Karran, P. DNA Mismatch Binding Defects, DNA Damage Tolerance, and Mutator Phenotypes in Human Colorectal Carcinoma Cell Lines. *Cancer Res.* **1995,** *55*, 2304–2309. (d) McFaline-Figueroa, J. L.; Braun, C. J.; Stanciu, M.; Nagel, Z. D.; Mazzucato, P.; Sangaraju, D.; Cerniauskas, E.; Barford, K.; Vargas, A.; Chen, Y.; Tretyakova, N.; Lees, J. A.; Hemann, M. T.; White, F. M.; Samson, L. D. Minor Changes in Expression of the Mismatch Repair Protein MSH2 Exert a Major Impact on Glioblastoma Response to Temozolomide. *Cancer Res.* **2015,** *75*, 3127–3138.
(20) Weller, M.; Le Rhun, E. How Did Lomustine Become Standard of Care in Recurrent Glioblastoma? *Cancer Treat. Rev.* **2020,** *87*, 102029.
(21) Wick, W.; Gorlia, T.; Bendszus, M.; Taphoorn, M.; Sahm, F.; Harting, I.; Brandes, A. A.; Taal, W.; Domont, J.; Idbaih, A.; Campone, M.; Clement, P. M.; Stupp, R.; Fabbro, M.; Le Rhun, E.; Dubois, F.; Weller, M.; von Deimling, A.; Golfinopoulos, V.; Bromberg, J. C.; Platten, M.; Klein, M.; van den Bent, M. J. Lomustine and Bevacizumab in Progressive Glioblastoma. *N. Engl. J. Med.* **2017,** *377*, 1954–1963.
(22) Tong, W. P.; Kirk, M. C.; Ludlum, D. B. Formation of the Cross-Link 1-[N3-Deoxycytidyl],2-[N1-Deoxyguanosinyl]-Ethane in DNA Treated with N,N′-Bis(2-Chloroethyl)-N-Nitrosourea. *Cancer Res.* **1982,** *42*, 3102–3105.

(23) Aquilina, G.; Ceccotti, S.; Martinelli, S.; Hampson, R.; Bignami, M. N-(2-Chloroethyl)-N′-Cyclohexyl-N-Nitrosourea Sensitivity in Mismatch Repair-Defective Human Cells. *Cancer Res.* **1998,** *58*, 135–141.
(24) For the initial discovery, mechanistic study, and in vitro and in vivo evaluation of KL-50 (**19**), see: Lin, K.; Gueble, S. E.; Sundaram, R. K.; Huseman, E. D.; Bindra, R. S.; Herzon, S. B. Mechanism-Based Design of Agents That Selectively Target Drug-Resistant Glioma. *Science* **2022,** *377*, 502–511.
(25) Le Rhun, E.; Oppong, F. B.; van den Bent, M.; Wick, W.; Brandes, A. A.; Taphoorn, M. J.; Platten, M.; Idbaih, A.; Clement, P. M.; Preusser, M.; Golfinopoulos, V.; Gorlia, T.; Weller, M. Thrombocytopenia Limits the Feasibility of Salvage Lomustine Chemotherapy in Recurrent Glioblastoma: A Secondary Analysis of EORTC 26101. *Eur. J. Cancer* **2023,** *178*, 13–22.
(26) (a) Gundersen, S.; Aamdal, S.; Fodstad, O. Mitozolomide (NSC 353451), a New Active Drug in the Treatment of Malignant Melanoma. Phase II Trial in Patients with Advanced Disease. *Br. J. Cancer* **1987,** *55*, 433–435. (b) Harding, M.; Northcott, D.; Smyth, J.; Stuart, N. S.; Green, J. A.; Newlands, E. Phase II Evaluation of Mitozolomide in Ovarian Cancer. *Br. J. Cancer* **1988,** *57*, 113–114. (c) Herait, P.; Rougier, P.; Oliveira, J.; Delgado, F. M.; May-Levin, F.; Hayat, M.; Armand, J. P. Phase II Study of Mitozolomide (M & B 39,565) in Colorectal and Breast Cancer. *Invest. New Drugs* **1988,** *6*, 323–325. (d) Blackledge, G.; Roberts, J. T.; Kaye, S.; Taylor, R.; Williams, J.; de Stavola, B.; Uscinska, B. A Phase II Study of Mitozolomide in Metastatic Transitional Cell Carcinoma of the Bladder. *Eur. J. Cancer Clin. Oncol.* **1989,** *25*, 391–392. (e) Herait, P.; Armand, J. P.; Benahmed, M.; Domenge, C.; Fontana, X.; Recondo, G.; Cvitkovic, E.; Delgado, F. M. Phase II Study of Mitozolomide (M & B 39,565) in Head and Neck Cancer. *Med. Oncol. Tumor Pharmacother.* **1989,** *6*, 267–269. (f) Neijt, J. P.; van der Burg, M. E.; Guastalla, J. P.; George, M.; Piccart, M.; Vermorken, J.; Carnino, F.; Rotmensz, N. Phase II Trial of Mitozolomide in Patients with Advanced Ovarian Cancer. A Study of the EORTC Gynecological Cancer Cooperative Group. *Acta Oncol.* **1989,** *28*, 663–665. (g) Smyth, J. F.; Gundersen, S.; Renard, J.; Pinedo, H. M. Randomized Phase II Trial of TCNU Versus Mitozolomide in Malignant Melanoma. EORTC Early Clinical Trials Group. *Eur. J. Cancer Clin. Oncol.* **1989,** *25*, 755–757. (h) van Oosterom, A. T.; Stoter, G.; Bono, A. V.; Splinter, T. A.; Fossa, S. D.; Verbaeys, A. J.; de Mulder, P. H.; de Pauw, M.; Sylvester, R. Mitozolomide in Advanced Renal Cancer. A Phase II Study in Previously Untreated Patients from the EORTC Genito-Urinary Tract Cancer Cooperative Group. *Eur. J. Cancer Clin. Oncol.* **1989,** *25*, 1249–1250.
(27) (a) Gibson, N. W.; Hickman, J. A.; Erickson, L. C. DNA Cross-Linking and Cytotoxicity in Normal and Transformed Human Cells Treated in Vitro with 8-Carbamoyl-3-(2-chloroethyl)imidazo[5,1-d]-1,2,3,5-tetrazin-4(3H)-one. *Cancer Res.* **1984,** *44*, 1772–1775. (b) Gibson, N. W.; Erickson, L. C.; Hickman, J. A. Effects of the Antitumor Agent 8-Carbamoyl-3-(2-chloroethyl)imidazo[5,1-d]-1,2,3,5-tetrazin-4(3H)-one on the DNA of Mouse L1210 Cells. *Cancer Res.* **1984,** *44*, 1767–1771.
(28) Erickson, L. C.; Bradley, M. O.; Ducore, J. M.; Ewig, R. A. G.; Kohn, K. W. DNA Crosslinking and Cytotoxicity in Normal and Transformed Human Cells Treated with Antitumor Nitrosoureas. *Proc. Natl. Acad. Sci. U.S.A.* **1980,** *77*, 467–471.
(29) Additionally, this data suggests the toxicity of lomustine (10) and MTZ (11) in the MGMT+ IR-90 cells was not the result of simple stoichiometry in which high doses of drug generated sufficient quantities of O6G adducts to exceed the repair capacity of MGMT, leading to ICL formation.
(30) Gibson, N. W.; Hickman, J. A. The Role of Isocyanates in the Toxicity of Antitumour Haloalkylnitrosoureas. *Biochem. Pharmacol.* **1982,** *31*, 2795–2800.
(31) Horgan, C. M.; Tisdale, M. J. Antitumour Imidazotetrazines--IV. An Investigation into the Mechanism of Antitumour Activity of a Novel and Potent Antitumour Agent, Mitozolomide (CCRG 81010, M & B 39565; NSC 353451). *Biochem. Pharmacol.* **1984,** *33*, 2185–2192.
(32) (a) Brent, T. P.; Smith, D. G.; Remack, J. S. Evidence That O^6-Alkylguanine-DNA Alkyltransferase Becomes Covalently Bound to DNA Containing 1,3-Bis(2-Chloroethyl)-1-Nitrosourea-Induced Precursors of Interstrand Cross-Links. *Biochem. Biophys. Res. Commun.* **1987,** *142*, 341–347. (b) Brent, T. P.; Remack, J. S.; Smith, D. G. Characterization of a Novel Reaction by Human O^6-Alkylguanine-DNA Alkyltransferase with 1,3-Bis(2-Chloroethyl)-1-Nitrosourea-Treated DNA. *Cancer Res.* **1987,** *47*, 6185–6188. (c) Brent, T. P.; Remack, J. S. Formation of Covalent Complexes between Human O^6-Alkylguanine-DNA Alkyltransferase and BCNU-Treated Defined Length Synthetic Oligodeoxynucleotides. *Nucleic Acids Res.* **1988,** *16*, 6779–6788.
(33) Gonzaga, P. E.; Potter, P. M.; Niu, T.-q.; Yu, D.; Ludlum, D. B.; Rafferty, J. A.; Margison, G. P.; Brent, T. P. Identification of the Cross-Link between Human O^6-Methylguanine-DNA Methyltransferase and Chloroethylnitrosourea-Treated DNA. *Cancer Res.* **1992,** *52*, 6052-6058.

(34) (a) Abril, N.; Luque-Romero, F. L.; Prieto-Alamo, M. J.; Rafferty, J. A.; Margison, G. P.; Pueyo, C. Bacterial and Mammalian DNA Alkyltransferases Sensitize *Escherichia coli* to the Lethal and Mutagenic Effects of Dibromoalkanes. *Carcinogenesis* **1997,** *18*, 1883–1888. (b) Liu, H.; Xu-Welliver, M.; Pegg, A. E. The Role of Human O^6-Alkylguanine-DNA Alkyltransferase in Promoting 1,2-Dibromoethane-Induced Genotoxicity in *Escherichia coli*. *Mutat. Res.* **2000,** *452*, 1–10. (c) Liu, L.; Pegg, A. E.; Williams, K. M.; Guengerich, F. P. Paradoxical Enhancement of the Toxicity of 1,2-Dibromoethane by O^6-Alkylguanine-DNA Alkyltransferase. *J. Biol. Chem.* **2002,** *277*, 37920–37928.
(35) Chowdhury, G.; Cho, S. H.; Pegg, A. E.; Guengerich, F. P. Detection and Characterization of 1,2-Dibromoethane-Derived DNA Crosslinks Formed with O^6-Alkylguanine-DNA Alkyltransferase. *Angew. Chem., Int. Ed. Engl.* **2013,** *52*, 12879–12882.
(36) Chesner, L. N.; Campbell, C. A Quantitative PCR-Based Assay Reveals That Nucleotide Excision Repair Plays a Predominant Role in the Removal of DNA-Protein Crosslinks from Plasmids Transfected into Mammalian Cells. *DNA Repair* **2018,** *62*, 18–27.
(37) Pegg, A. E.; Scicchitano, D.; Dolan, M. E. Comparison of the Rates of Repair of O^6-Alkylguanines in DNA by Rat Liver and Bacterial O^6-Alkylguanine-DNA Alkyltransferase. *Cancer Res.* **1984,** *44*, 3806–3811.
(38) Parker, S.; Kirk, M. C.; Ludlum, D. B. Synthesis and Characterization of O^6-(2-Chloroethyl)guanine: A Putative Intermediate in the Cytotoxic Reaction of Chloroethylnitrosoureas with DNA. *Biochem. Biophys. Res. Commun.* **1987,** *148*, 1124–1128.
(39) Ali-Osman, F.; Giblin, J.; Berger, M.; Murphy, M. J., Jr.; Rosenblum, M. L. Chemical Structure of Carbamoylating Groups and Their Relationship to Bone Marrow Toxicity and Antiglioma Activity of Bifunctionally Alkylating and Carbamoylating Nitrosoureas. *Cancer Res.* **1985,** *45*, 4185–4191.
(40) Tong, W. P.; Kirk, M. C.; Ludlum, D. B. Mechanism of Action of the Nitrosoureas—V. Formation of O^6-(2-Fluoroethyl)guanine and Its Probable Role in the Crosslinking of Deoxyribonucleic Acid. *Biochem. Pharmacol.* **1983,** *32*, 2011–2015.
(41) Pan, Y. The Dark Side of Fluorine. *ACS Med. Chem. Lett.* **2019,** *10*, 1016–1019.
(42) (a) Reynolds, C. H. Structure and Relative Stability of Halogenated Carbocations: The $C_2H_4X^+$ and $C_4H_8X^+$ (X = F, Cl, Br) Cations. *J. Am. Chem. Soc.* **1992,** *114*, 8676–8682. (b) Lown, J. W.; Singh, R. Synthesis of 3(2-Haloethyl)Aryltriazenes and Study of Their Reactions in Aqueous Solution. *Can. J. Chem.* **1981,** *59*, 1347–1356.
(43) Stevens, M. F. G.; Cousin, D.; Jennings, S.; McCarroll, A. J.; Williams, J. G.; Hummersone, M. G.; Zhang, J. Preparation of Oxodihydroimidazotetrazinecaboxylic Acid Derivatives for Use as Antiproliferative Agents. WO2009077741A2, 2009.
(44) Ege, G.; Gilbert, K. [7+2]- and [11+2]-Cycloaddition Reactions of Diazo-Azoles with Isocyanates to Azolo[5,1-d] [1,2,3,5] Tetrazine-4-ones. *Tetrahedron Lett.* **1979,** *20*, 4253–4256.
(45) (a) Stevens, M. F.; Hickman, J. A.; Stone, R.; Gibson, N. W.; Baig, G. U.; Lunt, E.; Newton, C. G. Antitumor Imidazotetrazines. 1. Synthesis and Chemistry of 8-Carbamoyl-3-(2-chloroethyl)Imidazo[5,1-d]-1,2,3,5-tetrazin-4(3 H)-one , a Novel Broad-Spectrum Antitumor Agent. *J. Med. Chem.* **1984,** *27*, 196–201. (b) Stevens, M. F. G.; Horspool, K. R.; Baig, G. U.; Lunt, E.; Newton, C. G.; Walsh, R. J. A. Preparation, Testing, and Formulation of Azolotetrazinones as Neoplasm Inhibitors and Immunosuppressants. EP252682A2, 1988.
(46) For discussions of the utility of isogenic cell line models, see: (a) Sajjad, H.; Imtiaz, S.; Noor, T.; Siddiqui, Y. H.; Sajjad, A.; Zia, M. Cancer Models in Preclinical Research: A Chronicle Review of Advancement in Effective Cancer Research. *Anim. Models Exp. Med.* **2021,** *4*, 87–103. (b) Feng, X.; Tang, M.; Dede, M.; Su, D.; Pei, G.; Jiang, D.; Wang, C.; Chen, Z.; Li, M.; Nie, L.; Xiong, Y.; Li, S.; Park, J.-M.; Zhang, H.; Huang, M.; Szymonowicz, K.; Zhao, Z.; Hart, T.; Chen, J. Genome-Wide CRISPR Screens Using Isogenic Cells Reveal Vulnerabilities Conferred by Loss of Tumor Suppressors. *Sci. Adv.* **2022,** *8*, eabm6638.
(47) (a) Yu, C.; Mannan, A. M.; Yvone, G. M.; Ross, K. N.; Zhang, Y. L.; Marton, M. A.; Taylor, B. R.; Crenshaw, A.; Gould, J. Z.; Tamayo, P.; Weir, B. A.; Tsherniak, A.; Wong, B.; Garraway, L. A.; Shamji, A. F.; Palmer, M. A.; Foley, M. A.; Winckler, W.; Schreiber, S. L.; Kung, A. L.; Golub, T. R. High-Throughput Identification of Genotype-Specific Cancer Vulnerabilities in Mixtures of Barcoded Tumor Cell Lines. *Nat Biotechnol* **2016,** *34*, 419–423. (b) Corsello, S. M.; Nagari, R. T.; Spangler, R. D.; Rossen, J.; Kocak, M.; Bryan, J. G.; Humeidi, R.; Peck, D.; Wu, X.; Tang, A. A.; Wang, V. M.; Bender, S. A.; Lemire, E.; Narayan, R.; Montgomery, P.; Ben-David, U.; Garvie, C. W.; Chen, Y.; Rees, M. G.; Lyons, N. J.; McFarland, J. M.; Wong, B. T.; Wang, L.; Dumont, N.; O'Hearn, P. J.; Stefan, E.; Doench, J. G.; Harrington, C. N.; Greulich, H.; Meyerson, M.; Vazquez, F.; Subramanian, A.; Roth, J. A.; Bittker, J. A.; Boehm, J. S.; Mader, C. C.; Tsherniak, A.; Golub, T. R. Discovering the Anticancer Potential of Non-Oncology Drugs by Systematic Viability Profiling. *Nat. Cancer* **2020,** *1*, 235–248.

(48) (a) Garnett, M. J.; Edelman, E. J.; Heidorn, S. J.; Greenman, C. D.; Dastur, A.; Lau, K. W.; Greninger, P.; Thompson, I. R.; Luo, X.; Soares, J.; Liu, Q.; Iorio, F.; Surdez, D.; Chen, L.; Milano, R. J.; Bignell, G. R.; Tam, A. T.; Davies, H.; Stevenson, J. A.; Barthorpe, S.; Lutz, S. R.; Kogera, F.; Lawrence, K.; McLaren-Douglas, A.; Mitropoulos, X.; Mironenko, T.; Thi, H.; Richardson, L.; Zhou, W.; Jewitt, F.; Zhang, T.; O'Brien, P.; Boisvert, J. L.; Price, S.; Hur, W.; Yang, W.; Deng, X.; Butler, A.; Choi, H. G.; Chang, J. W.; Baselga, J.; Stamenkovic, I.; Engelman, J. A.; Sharma, S. V.; Delattre, O.; Saez-Rodriguez, J.; Gray, N. S.; Settleman, J.; Futreal, P. A.; Haber, D. A.; Stratton, M. R.; Ramaswamy, S.; McDermott, U.; Benes, C. H. Systematic Identification of Genomic Markers of Drug Sensitivity in Cancer Cells. *Nature* **2012,** *483*, 570–575. (b) Iorio, F.; Knijnenburg, T. A.; Vis, D. J.; Bignell, G. R.; Menden, M. P.; Schubert, M.; Aben, N.; Goncalves, E.; Barthorpe, S.; Lightfoot, H.; Cokelaer, T.; Greninger, P.; van Dyk, E.; Chang, H.; de Silva, H.; Heyn, H.; Deng, X.; Egan, R. K.; Liu, Q.; Mironenko, T.; Mitropoulos, X.; Richardson, L.; Wang, J.; Zhang, T.; Moran, S.; Sayols, S.; Soleimani, M.; Tamborero, D.; Lopez-Bigas, N.; Ross-Macdonald, P.; Esteller, M.; Gray, N. S.; Haber, D. A.; Stratton, M. R.; Benes, C. H.; Wessels, L. F. A.; Saez-Rodriguez, J.; McDermott, U.; Garnett, M. J. A Landscape of Pharmacogenomic Interactions in Cancer. *Cell* **2016,** *166*, 740–754. (c) Picco, G.; Chen, E. D.; Alonso, L. G.; Behan, F. M.; Goncalves, E.; Bignell, G.; Matchan, A.; Fu, B.; Banerjee, R.; Anderson, E.; Butler, A.; Benes, C. H.; McDermott, U.; Dow, D.; Iorio, F.; Stronach, E.; Yang, F.; Yusa, K.; Saez-Rodriguez, J.; Garnett, M. J. Functional Linkage of Gene Fusions to Cancer Cell Fitness Assessed by Pharmacological and CRISPR-Cas9 Screening. *Nat. Commun.* **2019,** *10*, 2198. (d) DepMap, Broad (2023): This DepMap release contains data from CRISPR knockout screens from project Achilles, as well as genomic characterization data from the CCLE project. For more information, please see README.txt.. figshare. Dataset. https://doi.org/10.6084/m9.figshare.22765112.v2

(49) (a) McKenna, D. J.; Gallus, M.; McKeown, S. R.; Downes, C. S.; McKelvey-Martin, V. J. Modification of the Alkaline Comet Assay to Allow Simultaneous Evaluation of Mitomycin C-Induced DNA Cross-Link Damage and Repair of Specific DNA Sequences in RT4 Cells. *DNA Repair* **2003,** *2*, 879–890. (b) Wu, J. H.; Jones, N. J. Assessment of DNA Interstrand Crosslinks Using the Modified Alkaline Comet Assay. *Methods Mol. Biol.* **2012,** *817*, 165–181.

(50) For a review on the Fanconi anaemia pathway, see: Ceccaldi, R.; Sarangi, P.; D'Andrea, A. D. The Fanconi Anaemia Pathway: New Players and New Functions. *Nat. Rev. Mol. Cell Biol.* **2016,** *17*, 337–349.

(51) (a) Bodell, W. J.; Pongracz, K. Chemical Synthesis and Detection of the Cross-Link 1-[N^3-(2′-Deoxycytidyl)]-2-[N^1-(2′-deoxyguanosinyl)]ethane in DNA Reacted with 1-(2-Chloroethyl)-1-nitrosourea. *Chem. Res. Toxicol.* **1993,** *6*, 434-438. (b) Bai, B.-Q.; Zhao, L.-J.; Song, X.-Q.; Zhong, R.-G. Synthesis of 1-[N-(2′-deoxycytidyl)]-2-[N-(2′-deoxyguanosyl)]ethane and Its Application in the Detection of DNA Interstrand Crosslink. *Hecheng Huaxue* **2010,** *18*, 280–284.

(52) (a) Fischhaber, P. L.; Gall, A. S.; Duncan, J. A.; Hopkins, P. B. Direct Demonstration in Synthetic Oligonucleotides That *N*,*N′*-Bis(2-chloroethyl)-nitrosourea Cross-Links N^1 of Deoxyguanosine to N^3 of Deoxycytidine on Opposite Strands of Duplex DNA. *Cancer Res.* **1999,** *59*, 4363–4368. (b) Bai, B.-Q.; Zhao, L.-J.; Zhong, R.-G. Analysis of Deoxyribonucleic Acid Interstrand Cross-Links Induced by Nitrosourea with High Performance Liquid Chromatography-Electrospray Ionization Tandem Mass Spectrometry. *Chinese J. Anal. Chem.* **2010,** *38*, 532–536.

(53) (a) Shibata, T.; Williams, D. M. Novel Post DNA Synthesis Chemistry for Preparing Oligonucleotides Containing O6-Modified Purines. *Nucleic Acids Symp. Ser.* **2005**, 23–24. (b) Shibata, T.; Glynn, N.; McMurry, T. B.; McElhinney, R. S.; Margison, G. P.; Williams, D. M. Novel Synthesis of O^6-Alkylguanine Containing Oligodeoxyribonucleotides as Substrates for the Human DNA Repair Protein, O^6-Methylguanine DNA Methyltransferase (MGMT). *Nucleic Acids Res.* **2006,** *34*, 1884–1891. (c) Millington, C. L.; Watson, A. J.; Marriott, A. S.; Margison, G. P.; Povey, A. C.; Williams, D. M. Convenient and Efficient Syntheses of Oligodeoxyribonucleotides Containing O^6-(Carboxymethyl)guanine and O^6-(4-Oxo-4-(3-[yridyl)butyl)guanine. *Nucleosides Nucleotides Nucleic Acids* **2012,** *31*, 328–338.

(54) Hentschel, S.; Alzeer, J.; Angelov, T.; Scharer, O. D.; Luedtke, N. W. Synthesis of DNA Interstrand Cross-Links Using a Photocaged Nucleobase. *Angew. Chem., Int. Ed. Engl.* **2012,** *51*, 3466–3469.

(55) Engels, J. W.; Hofmann, T.; Zweig, K. A New Synthetic Approach for the Synthesis of N^2-Modified Guanosines. *Synthesis* **2005,** *2005*, 1797–1800.

(56) Pletsas, D.; Wheelhouse, R. T.; Pletsa, V.; Nicolaou, A.; Jenkins, T. C.; Bibby, M. C.; Kyrtopoulos, S. A. Polar, Functionalized Guanine-*O*6 Derivatives Resistant to Repair by *O*6-Alkylguanine-DNA Alkyltransferase: Implications for the Design of DNA-Modifying Drugs. *Eur. J. Med. Chem.* **2006,** *41*, 330–339.
(57) Bonala, R. R.; Torres, M. C.; Attaluri, S.; Iden, C. R.; Johnson, F. Incorporation of N^2-Deoxyguanosine Metabolic Adducts of 2-Aminonaphthalene and 2-Aminofluorene into Oligomeric DNA. *Chem. Res. Toxicol.* **2005,** *18*, 457–465.
(58) Okamoto, A.; Tanaka, K.; Saito, I. A Nucleobase That Releases Reporter Tags upon DNA Oxidation. *J. Am. Chem. Soc.* **2004,** *126*, 416–417.
(59) Gillet, L. C.; Alzeer, J.; Scharer, O. D. Site-Specific Incorporation of *N*-(Deoxyguanosin-8-yl)-2-acetylaminofluorene (dG-AAF) into Oligonucleotides Using Modified 'Ultra-Mild' DNA Synthesis. *Nucleic Acids Res.* **2005,** *33*, 1961–1969.
(60) Pon, R. T.; Yu, S. Hydroquinone-*O*,*O'*-Diacetic Acid ('Q-Linker') as a Replacement for Succinyl and Oxalyl Linker Arms in Solid Phase Oligonucleotide Synthesis. *Nucleic Acids Res.* **1997,** *25*, 3629–3635.
(61) Kohn, W.; Sham, L. J. Self-Consistent Equations Including Exchange and Correlation Effects. *Physical Review* **1965,** *140*, A1133-A1138.
(62) Klan, P.; Solomek, T.; Bochet, C. G.; Blanc, A.; Givens, R.; Rubina, M.; Popik, V.; Kostikov, A.; Wirz, J. Photoremovable Protecting Groups in Chemistry and Biology: Reaction Mechanisms and Efficacy. *Chem. Rev.* **2013,** *113*, 119–191.
(63) (a) Wu, R. S.; Hurst-Calderone, S.; Kohn, K. W. Measurement of O^6-Alkylguanine-DNA Alkyltransferase Activity in Human Cells and Tumor Tissues by Restriction Endonuclease Inhibition. *Cancer Res.* **1987,** *47*, 6229–6235. (b) Encell, L. P.; Loeb, L. A. Redesigning the Substrate Specificity of Human O^6-Alkylguanine-DNA Alkyltransferase. Mutants with Enhanced Repair of O^4-Methylthymine. *Biochem.* **1999,** *38*, 12097–12103.
(64) Dolan, M. E.; Pegg, A. E. O^6-Benzylguanine and Its Role in Chemotherapy. *Clin. Cancer Res.* **1997,** *3*, 837–847.
(65) Zhao, L.; Li, L.; Xu, J.; Zhong, R. Comparative Investigation of the DNA Inter-Strand Crosslinks Induced by ACNU, BCNU, CCNU and FTMS Using High-Performance Liquid Chromatography–electrospray Ionization Tandem Mass Spectrometry. *Int. J. Mass Spectrum.* **2014,** *368*, 30–36.
(66) Wheeler, J. B.; Stourman, N. V.; Armstrong, R. N.; Guengerich, F. P. Conjugation of Haloalkanes by Bacterial and Mammalian Glutathione Transferases: Mono- and Vicinal Dihaloethanes. *Chem. Res. Toxicol.* **2001,** *14*, 1107–1117.
(67) Humphreys, W. G.; Kim, D. H.; Cmarik, J. L.; Shimada, T.; Guengerich, F. P. Comparison of the DNA-Alkylating Properties and Mutagenic Responses of a Series of *S*-(2-Haloethyl)-Substituted Cysteine and Glutathione Derivatives. *Biochem.* **1990,** *29*, 10342–10350.
(68) Fan, C. H.; Liu, W. L.; Cao, H.; Wen, C.; Chen, L.; Jiang, G. O^6-Methylguanine DNA Methyltransferase as a Promising Target for the Treatment of Temozolomide-Resistant Gliomas. *Cell Death Dis.* **2013,** *4*, e876.
(69) Jiménez-Alcázar, M.; Curiel-García, Á.; Nogales, P.; Perales-Patón, J.; Schuhmacher, A. J.; Galán-Ganga, M.; Zhu, L.; Lowe, S. W.; Al-Shahrour, F.; Squatrito, M. Dianhydrogalactitol Overcomes Multiple Temozolomide Resistance Mechanisms in Glioblastoma. *Mol. Cancer Ther.* **2021,** *20*, 1029–1038.
(70) (a) Pletsas, D.; Garelnabi, E. A. E.; Li, L.; Phillips, R. M.; Wheelhouse, R. T. Synthesis and Quantitative Structure–Activity Relationship of Imidazotetrazine Prodrugs with Activity Independent of *O*6-Methylguanine-DNA-methyltransferase, DNA Mismatch Repair, and p53. *J. Med. Chem.* **2013,** *56*, 7120–7132. (b) Svec, R. L.; McKee, S. A.; Berry, M. R.; Kelly, A. M.; Fan, T. M.; Hergenrother, P. J. Novel Imidazotetrazine Evades Known Resistance Mechanisms and Is Effective against Temozolomide-Resistant Brain Cancer in Cell Culture. *ACS Chem. Biol.* **2022,** *17*, 299–313.
(71) (a) Day, R. S., 3rd; Ziolkowski, C. H.; Scudiero, D. A.; Meyer, S. A.; Mattern, M. R. Human Tumor Cell Strains Defective in the Repair of Alkylation Damage. *Carcinogenesis* **1980,** *1*, 21–32. (b) Day, R. S.; Ziolkowski, C. H. J.; Scudiero, D. A.; Meyer, S. A.; Lubiniecki, A. S.; Girardi, A. J.; Galloway, S. M.; Bynum, G. D. Defective Repair of Alkylated DNA by Human Tumour and SV40-Transformed Human Cell Strains. *Nature* **1980,** *288*, 724–727.

For Table of Contents Only: